C. R. Palevol 15 (2016) 176–196

Contents lists available at ScienceDirect

Comptes Rendus Palevol

www.sciencedirect.com

General Palaeontology, Systematics and Evolution (Palaeohistology)

Mineralized tissues in dinosaurs interpreted as having formed through metaplasia: A preliminary evaluation

La métaplasie interprétée comme un processus de formation de certains tissus minéralisés de dinosaures : une évaluation préliminaire

John R. Horner[a,b,*], Holly N. Woodward[a,c], Alida M. Bailleul[a,b]

[a] *Museum of the Rockies, Montana State University, Bozeman, MT 59717, USA*
[b] *Department of Earth Sciences, Montana State University, Bozeman MT 59715, USA*
[c] *Department of Anatomy and Cell Biology, Oklahoma State University Center for Health Sciences, Tulsa, OK 74107, USA*

ARTICLE INFO

Article history:
Received 1st December 2014
Accepted after revision 22 January 2015
Available online 15 April 2015

Handled by Michel Laurin

Keywords:
Metaplasia
"Ossified" tendons
Dinosauria
Ornithischia
Saurischia
Aves
Alternative mode of "ossification"

ABSTRACT

Evolutionary biologists define "metaplasia" as the permanent transformation of a cell identity, and there are many examples of such transformations in living vertebrates (e.g., chondrocytes transforming directly into osteoblasts). These metaplasias have been observed during the mineralization of "ossified" tendons of living birds. In the present study, we examined "ossified" tendons in *Bubo* and *Meleagris* and used the characteristics of these metaplastic tissues to recognize them in several non-avian dinosaur taxa. The fossilized skeletal elements that form our sample are varied and include hadrosaurian tendons and a nasal bone, an ankylosaur tail club "handle", sauropod neural spines, and some dromaeosaur tail rods. The extant avian mineralized tendons were formed of a primary tissue (analogous to primary bone) and secondary reconstructions (SRs; analogous to secondary osteons). Both were composed of fiber bundles (or fascicles) that were closely packed together and separated by arc-shaped spaces in cross-section. When viewed longitudinally, they were arranged in a herringbone pattern. There is no evidence of osteocytes within the primary tendon matrix; what was previously interpreted as osteocyte lacunae are instead arc-shaped spaces between fiber fascicles, and tissue immediately surrounding vascular spaces is dense, avascular and apparently hypermineralized. Mineralization of fibers began centrally and moved in a centrifugal direction. In the non-avian dinosaurs examined, primary and secondary tissue structures were virtually identical to those found within the avian mineralized tendons. Indeed, (1) they were densely fibrous; (2) they showed fiber fascicles separated by arcuate-shaped spaces when viewed transversally, and (3) they were arranged in a herringbone pattern longitudinally. SRs differ from typical Haversian systems in possessing highly irregular borders, suggesting destruction of the fibrous matrix and formation of initial vascular spaces was accomplished perhaps by phagocytosis or enzymatic lysis with subsequent remodeling by fibrocytes, fibroblasts, or an as of yet unknown cell type. Osteocytes with canaliculi were only observed in "mature" SRs, found deep within the elements (and never close to their external borders). Because fossilized primary and secondary tissue structures were identical to those found within the avian mineralized tendons examined, it is likely that identical processes are responsible for their formation. Biomechanical properties were also likely similar, potentially affording carbon fiber-like, trauma-resistant properties to the "ossified" tendons and nasal bones of hadrosaurs, the tail "handles" of ankylosaurs, and the tail rods of dromaeosaurs. In contrast, the primary

* Corresponding author.
E-mail address: jhorner@montana.edu (J.R. Horner).

http://dx.doi.org/10.1016/j.crpv.2015.01.006

tissue from a sauropod mineralized nuchal ligament appears to be made of hypermineralized fibrocartilage, but the SRs interdigitating with the hypermineralized fibrocartilage resemble the reconstructions observed in the other fossil skeletal elements and likely formed by the same processes. Since no osteocyte lacunae were observed in any of these dinosaurian primary tissues, we hypothesize that the fossilized cranial and skeletal elements examined here formed through metaplastic transformation (perhaps from fibroblasts) rather than by periosteal and intramembranous ossification. This study suggests that alternative modes of mineralization might be more abundant in non-avian dinosaurs than previously reported.

Mots clés :
Métaplasie
Tendons « ossifiés »
Dinosauria
Ornithischia
Saurischia
Aves
Mode d'ossification alternatif

RÉSUMÉ

Les biologistes évolutionnistes définissent la « métaplasie » comme la transformation permanente de l'identité d'une cellule, et il existe beaucoup d'exemples de ce type de transformation chez les vertébrés actuels (par exemple, des chondrocytes qui se transforment en ostéoblastes). Ces métaplasies ont été observées pendant la minéralisation des tendons « ossifiés » d'oiseaux actuels. Dans cette étude, nous avons examiné des tendons ossifiés de *Bubo* et *Meleagris*, et utilisé les caractéristiques de leurs tissus métaplastiques pour reconnaître ces derniers chez plusieurs dinosaures non aviens. Les éléments fossilisés qui composent notre échantillon sont variés et incluent des tendons et un os nasal d'hadrosaure, la base de la massue de la queue d'un ankylosaure, des épines neurales de sauropodes et des apophyses allongées de vertèbres caudales de dromaeosaures. Les tendons minéralisés aviens montrent un tissu primaire (analogue à celui de l'os primaire) et des reconstructions secondaires (RSs ; analogues aux ostéones secondaires). Ces deux tissus sont composés de faisceaux fibreux qui sont très compactés et séparés par des espaces en forme d'arcs en section transversale. Lorsqu'ils sont observés longitudinalement, ces faisceaux forment des stratifications en arêtes de poissons (*herringbone*). Il n'y a aucune évidence d'ostéocytes au niveau de ce tissu primaire, et les espaces précédemment interprétés comme des lacunes ostéocytaires sont en fait simplement des espaces vides entre les faisceaux fibreux. Le tissu qui entoure les espaces vasculaires est dense, non vascularisé et apparemment hyperminéralisé. La minéralisation des fibres se fait de façon centrifuge. Chez les dinosaures non aviens, les structures primaires et secondaires sont identiques à celles trouvées dans les tendons minéralisés aviens. En effet, (1) ils sont très fibreux ; (2) ils ont des faisceaux fibreux séparés par des espaces en forme d'arc en section transversale, et (3) ils sont disposés en arêtes de poisson (*herringbone*) en vue longitudinale. Les RSs sont différentes des systèmes haversiens typiques, car elles possèdent des bords irréguliers, ce qui suggère une destruction de la matrice fibreuse et la formation d'espaces vasculaires initiaux (peut-être due à une lyse enzymatique ou une phagocytose). Par la suite, des fibroblastes, fibrocytes ou autres cellules auraient pris part au remodelage. Des ostéocytes avec des canalicules ont été observés uniquement dans des RSs matures, localisées profondément dans les éléments (et non au niveau de leurs bordures extérieures). Comme les tissus primaires et secondaires des fossiles sont identiques à ceux trouvés dans les tendons minéralisés d'oiseaux actuels, il est probable que des processus similaires sont responsables de la formation de ces éléments fossiles. Leurs propriétés biomécaniques étaient aussi vraisemblablement similaires, présentant peut-être une résistance aux traumatismes, comme la fibre de carbone. Même si le tissu primaire de l'épine neurale du sauropode est différent des autres tissus et semble être formé de fibrocartilage hyperminéralisé, ces RSs sont similaires à celles observées chez les autres dinosaures. Puisqu'aucune lacune ostéocytaire n'a été observée dans ces tissus primaires de dinosaures, nous formons l'hypothèse que ces tissus fossilisés ont étés formés par transformations métaplastiques (peut-être à partir de fibroblastes), plutôt que par ossification périostique et intramembranaire. Cette étude suggère que des modes de minéralisation alternatifs auraient pu être plus abondants chez les dinosaures non aviens que ce qui est généralement accepté.

1. Introduction

"Metaplastic bone", as described by Haines and Mohuiddin (1968), is a hard skeletal tissue formed in the absence of osteoblasts through a direct transformation of one tissue type to another. Unfortunately, the meaning behind terms "metaplasia" and "metaplastic bone" can be ambiguous because medical biologists and evolutionary biologists (including paleohistologists) use the terms differently.

For medical biologists, metaplasia is a *reversible* change in the structure and/or the secretion of a cell. As an example, we can cite the pseudostratified epithelium of the airways that becomes a squamous epithelium when exposed to cigarette smoke (e.g., Araya et al., 2007). On the other hand, evolutionary biologists define, "metaplasia" as the **permanent** transformation of a cell identity (Beresford, 1981; Hall, 2005). For evolutionary biologists, the cigarette example is identified as a "modulation" or "modulation of cellular activity" (see Chapter 5 in Hall, 2005), not "metaplasia". Using the evolutionary biology definition, many examples of metaplasias are recognized in extant vertebrates, such as chondrocytes transforming directly into osteoblasts in turtle and lizard limb bones (Haines, 1969 and the see other examples in the following paragraph). Permanent transformation of a cell identity is called "transdifferentiation" by medical biologist (e.g., Eguchi, 1976).

The purpose of this study is to demonstrate the prevalence of tissues that we interpret as metaplastic within various skeletal elements of selected non-avian dinosaur taxa. To do this, we use the evolutionary biology definition of "metaplasia": *permanent* transformation of one cell type into another, which in turn leads to a transformation of the tissue type. In addition, we assert that mineralization may or may not follow metaplasia. We think that our addendum completes the aforementioned definition from Haines and Mohuiddin (1968) concerning metaplastic "bone".

With regard to metaplastic "bone", two forms of metaplastic mineralization have been described (see Beresford, 1981; Francillon-Vieillot et al., 1990; Reid, 1996); one involves transformation from cartilage to a mineralized tissue (intracartilaginous), and the other involves a transformation from preformed dense connective tissues to a mineralized tissue (intratendinous). Intracartilaginous metaplastic tissue is only known from mammal epiphyses (Reid, 1996), while intratendinous metaplastic tissues reportedly form at least some portions of reptilian osteoderms (e.g., Levrat-Calviac and Zylberberg, 1986; Main et al., 2005; Moss, 1969; de Ricqlès et al., 2001; Scheyer and Sander, 2004; Vickaryous and Hall, 2008), portions of turtle shell (Scheyer et al., 2007), ossified tendons (Adams and Organ, 2005), cervical ribs (Cerda, 2009; Klein et al., 2012), possibly cranial elements (Goodwin and Horner, 2004; Horner and Goodwin, 2009; Horner and Lamm, 2011) and interspinous ligament scars (Reid, 1996). Metaplastic tissues also make up various parts of the avian skeleton (see Landis and Silver, 2002; Organ and Adams, 2005; Vanden Berge and Storer, 1995).

Regarding tissue mineralization, we quote Rooney (1994, p. 53): "A distinction must be made between ossification and mineralization. Although both processes involve the deposition of hydroxyapatite crystals, usually within a collagen-based extracellular matrix, ossification requires the initial presence of osteoblasts and the continued presence of osteocytes". From here on, we refer to the hard tissues hypothesized to have formed through metaplasia as mineralized tissues or metaplastic tissues rather than "metaplastic bone" contra Haines and Mohuiddin (1968), because these tissues do not contain the features characteristic of bone. We also remind the reader that in order to be preserved in the first place, all non-avian dinosaur tissues described herein must have been mineralized prior to death and subsequent fossilization. Thus, although we argue that the described dinosaur tissues in this study are the result of cellular metaplasia, we lack fossilized examples of the non-mineralized precursor tissues and the cells from which the mineralized tissues could have been derived. It is highly suspected that fibroblast-like cells transform directly into osteoblast-like cells (Matthew Vickaryous, *personal communication*), but alas, this cannot be confirmed in the present study. Instead, our primary focus here is describing metaplastic features at the histological level and not the cellular level.

To identify these potential tissues in dinosaurs, we relied on comparative morphology. For comparison, we used previously prepared and published ossified tendons of a turkey and Great Horned owl (see Organ and Adams, 2005) because avian ossified tendons are confirmed to mineralize through the process of metaplasia, as thoroughly described by Landis (1986) and Landis and Silver (2002). They were not chosen to imply a phylogenetic connection.

2. Materials and methods

Thin sections of numerous dinosaurian skeletal elements were examined for histologic tissues resembling those present in the avian ossified tendons. The taxa surveyed included tyrannosaurids, ceratopsids, pachycephalosaurids, hadrosaurids, thyreophorans, sauropods, and a dilophosaurid. The specimens described in this study represent only the skeletal elements found to have histologic tissues arguably similar to the avian tendons.

Specimens described and illustrated in this study include the tendons from two avian taxa (*Bubo* and *Meleagris*) used for comparison and a variety of dinosaurian skeletal elements from seven taxa (*Maiasaura*, *Brachylophosaurus*, *Deinonychus*, *Euoplocephalus*, *Sauropelta*, *Prosaurolophus*, and *Diplodocus*) (Table 1). All of the thin sections from fossil specimens were prepared in the Gabriel Laboratory for Cellular and Molecular Paleontology following the techniques of Horner and Lamm (2011) and Lamm (2013). All histological photographs were taken on a Nikon eclipse E600pol microscope with a Nikon Digital Sight DS-L1 camera system. Whole slide images (e.g. Fig. 4A) were digitized on a Canon Canoscan 8800F flatbed scanner.

The avian thin sections were prepared for a previous project in 2004, under the direction of Organ and Adams (see Adams and Organ, 2005; Organ and Adams, 2005). The "ossified" tendon derived from the M. *extensor carpi radialis* of *Bubo virginianus* (Great Horned owl; MOR 2001-10R) (MOR.H.2001-10R-Ten5-2, MOR.2001-10R-Ten4-2) (Fig. 1A–E) was sectioned transversely and stained with toluidine blue (see Organ and Adams, 2005), and an "ossified" tendon from the *M. fibularis longus* of *Meleagris gallopavo* (turkey; MOR.VR1315) was sectioned both transversely (MOR.VR1315-02-5T, MOR.VR1315-Ten1T) and longitudinally (MOR.VR1315-02-3T) (Fig. 1F–H), and stained with hematoxylin and eosin (H&E) (see Organ and Adams, 2005).

The bundle of tiny "ossified" tendons in Fig. 2A–C (MOR-GS400; MOR-GS400.OSS-440-4) was found in association

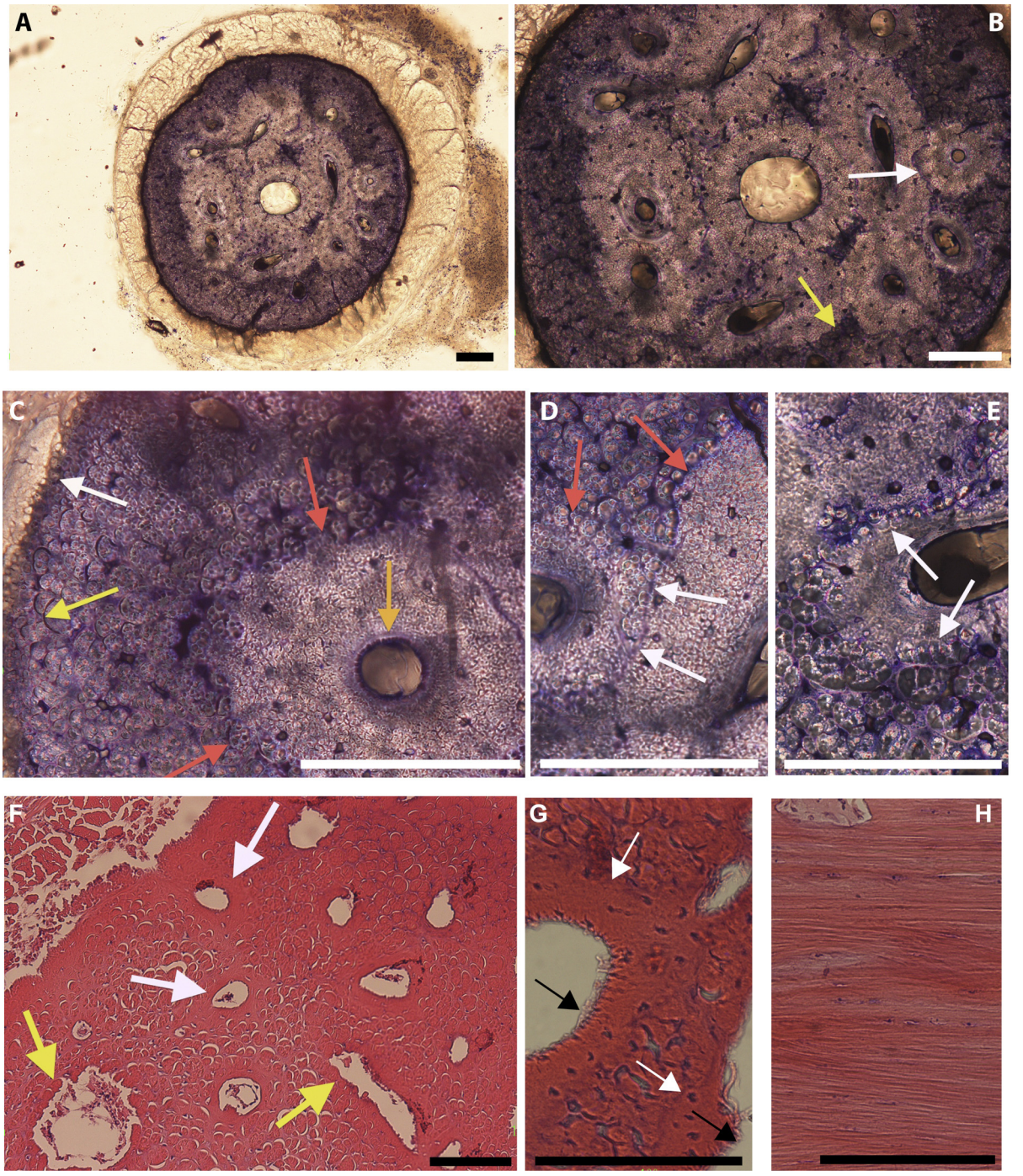

Fig. 1. (Color online.) Mineralized tendons of *Bubo virginianus* (MOR.H.2001-10R) (A–E), and *Meleagris gallopavo* (MOR.VR1315) (F–G). A. Transverse section of a tendon from the *M. extensor carpi radialis* encased within its paratenon (surrounding white structure). Tissues stained blue and purple are mineralized. B. Close-up of A, showing the boundaries of secondary reconstructive structures that have altered the central regions of the mineralized tendon. Note the coloration break between primary tissue and "secondary" tissue (yellow arrow) and that like Haversian systems, these features appear to invade previously formed systems giving the appearance of overlapping the older structures (white arrow). C. Outer area of the tendon showing individual collagen fibrils at the mineralization border (white arrow), arc-shaped space surrounding a fascicle (yellow arrow), the ragged, non-distinct boundary of a secondary reconstruction (red arrows), and the border tissue of a vascular canal hypothesized to be hypermineralized (orange arrow). D. Indistinct boundary of two secondary reconstructions (red arrows) showing that the border of the fascicles, as they are incorporated into a secondary reconstruction, forms a scalloped appearance. The white arrows point out the line between two secondary reconstructions and show that there is no evidence of resorption at this union. E. Boundary of a secondary reconstruction showing what appears to be the deconstruction of fascicle endotenons (arrows). F. Transverse section showing vascular spaces within the *Meleagris* tendon. The yellow arrows point out two vascular spaces with little or no surrounding reconstructive tissues, and the white arrows show vascular spaces that do have surrounding reconstructive tissues. Note that the outer edges of the reconstructive tissues are obscure and

Table 1
List of taxa, skeletal elements, slide orientation, and slide numbers, used in this study with figure references.
Tableau 1
Liste des taxons, des éléments squelettiques, des orientations des coupes et des numéros de coupes utilisés dans cette étude (avec référence aux figures).

Taxon	Specimen number	Skeletal element	Slice orientation	Slide ID	Figure
Bubo	MOR 2001-10R	*M. extensor carpi radialis* tendon	Transverse	MOR.2001-10R-Ten5-2	Fig. 1A, B, D, E
			Transverse	MOR.2001-10R-Ten4-2	Fig. 1C
Meleagris	MOR.VR1315	*M. extensor carpi radialis* tendon	Transverse	MOR.VR1315-02-5T	Fig. 1F
			Transverse	MOR.VR1315-Ten1T	Fig. 1G
			Longitudinal	MOR.VR1315-02-3T	Fig. 1H
Maiasaura	MOR-GS400	"Ossified" tendons	Frontal	MOR-GS400.OSS-440-4	Fig. 2A–C
Brachylophosaurus	MOR 794	"Ossified" tendon	Frontal	MOR794.OT1-A-1	Fig. 2D
			Rostro-caudal	MOR794.OT4-A-L1	Fig. 2G
			Frontal	MOR1071.Ten1-3	Fig. 2E, F
Deinonychus	MOR 747	Prezygopophyseal rods	Frontal	MOR747.Ten1-2	Fig. 3A, B
			Frontal	MOR747.Ten1-3A	Fig. 3C
			Frontal	MOR747.Ten1-1	Fig. 3D
			Frontal	MOR747.Ten1-2A	Fig. 3E
			Rostro-caudal	MOR747.Ten1-L2	Fig. 3F, G
Euoplocephalus	MOR 2010-09	Pre-club, tail complex	Frontal	MOR.2010-09.TC1-2	Fig. 4A–E
			Rostro-caudal	MOR.2010-09.TC1-L2	Fig. 4F
Sauropelta	MOR 3080	Osteoderm	Perpendicular to spike	MOR3080.Scu1-2	Fig. 5A–D, F, G
			Perpendicular to spike	MOR3080.Scu1-1	Fig. 5E
Prosaurolophus	MOR 553PN	Nasal	Frontal	MOR553PN.N1-2	Fig. 6A, C–F
			Coronal	MOR553PN.N1-1	Fig. 6B
			Rostro-caudal	MOR553PN.N1-L2	Fig. 6G
Diplodocus	MOR 592	Caudal neural spine	Transverse	MOR592.NS1-2	Fig. 7A–E, G
			Sagittal	MOR592.NS1-L1	Fig. 7F
		Caudal neural spine	Frontal	MOR592.NS1-L3	Fig. 8A, B, E, G; Fig. 9A–F
		Caudal neural spine	Frontal	MOR592.NS1-L6	Fig. 8C
		Caudal neural spine	Frontal	MOR592.NS1-L4	Fig. 8D, F

with a group of 15 small juvenile hadrosaurs referred to as *Maiasaura peeblesorum* (Horner and Makela, 1979). The location of the tendons in relationship to the skeleton is unknown, but they were sectioned frontally. An ossified tendon from an adult *Brachylophosaurus* (MOR 794) was also sectioned frontally (MOR794-OT1-A-1) as well as rostro-caudally (MOR794-OT4-A-L1) (Fig. 2D–F).

The prezygopophyseal tail rods of *Deinonychus antirrhopus* (Fig. 3) (MOR 747) were sectioned from an isolated fragment of distal caudal vertebra found in association with a group of *Deinonychus* skeletons, from the site originally described by Ostrom (1969). The exact caudal position is unknown. Frontal sections (MOR 747.Ten1-1, MOR 747.Ten1-2, MOR 747.Ten1-3A) were removed at either the anterior or posterior end of the vertebra, and a rostro-caudal section was taken from a medial position (MOR 747.Ten1-L2).

The tail club of *Euoplocephalus* (MOR 2010-09; TC1-2, TC1-L2) is a caudal vertebral complex composed of co-ossified centra together with elongated pre- and postzygopophyses, modified chevrons and a terminally enlarged "club" (see Coombs, 1995; Parks, 1924). For this study, we sectioned a partial "handle" (see terminology of Coombs, 1995) of cf. *Euoplocephalus* from the upper Two Medicine Formation (Campanian) of Montana. The specimen was crushed postmortem and is incomplete. The section (MOR.2010-09-TC) appears to consist of a portion of the centrum and some fused "ossified" tendons from a lateral position (Fig. 4). The sample was sectioned both frontally and rostro-caudally.

difficult to trace. G. A highly magnified image showing the indistinct outer borders of the secondary reconstructions (white arrows), and the fibrous borders of the inner rims of the vascular canals (black arrows). H. A longitudinal section of *Meleagris*, showing a herringbone pattern of mineralized collagen fibers. All scale bars are 100 μm.

Fig. 1. (Couleur en ligne.) Tendons minéralisés de *Bubo virginianus* (MOR.H.2001-10R) (A–E), et *Meleagris gallopavo* (MOR.VR1315) (F–G). A. Section transverse d'un tendon de *M. extensor carpi radialis* qui est logé dans son paratenon (structure extérieure blanche). Les tissus colorés en bleu et violet sont minéralisés. B. Agrandissement de A montrant les limites des reconstructions secondaires (RSs) qui ont altéré les régions centrales du tendon minéralisé. À noter la différence de coloration entre le tissu primaire et le tissu secondaire (flèches jaunes) et que, comme les systèmes haversiens, ces structures empiètent sur d'autres systèmes plus anciens (flèche blanche). C. Les aires extérieures du tendon montrent des fibres de collagène individuelles au niveau du bord de la minéralisation (flèche blanche), des espaces en forme d'arc entourant les faisceaux (flèche jaune), la limite indistincte d'une RS (flèches rouges) et un tissu entourant un canal vasculaire qui pourrait être hyperminéralisé (flèche orange). D. Limite indistincte de deux RSs (flèches rouges) montrant que les bords des faisceaux sont ondulés lorsqu'ils sont incorporés dans une RS. Les flèches blanches montrent la limite entre deux RSs, et n'indiquent aucune évidence de résorption. E. Limite d'une RS montrant une déconstruction d'endotenon de faisceaux (flèches). F. Section transverse montrant des espaces vasculaires au niveau du tendon de *Meleagris*. Les flèches jaunes indiquent deux espaces vasculaires avec très peu de tissus reconstructeurs, et les flèches blanches montrent des espaces vasculaires présentant ces tissus reconstructeurs. Notez que les bords extérieurs de ces tissus sont flous et difficiles à tracer. G. Image à fort grossissement montrant les bordures extérieures indistinctes des RSs (flèches blanches) et les bordures fibreuses de l'intérieur des canaux vasculaires (flèches noires). H. Section longitudinale de *Meleagris* montrant une organisation en arêtes de poisson des fibres minéralisées de collagène. Toutes les barres d'échelle représentent 100 μm.

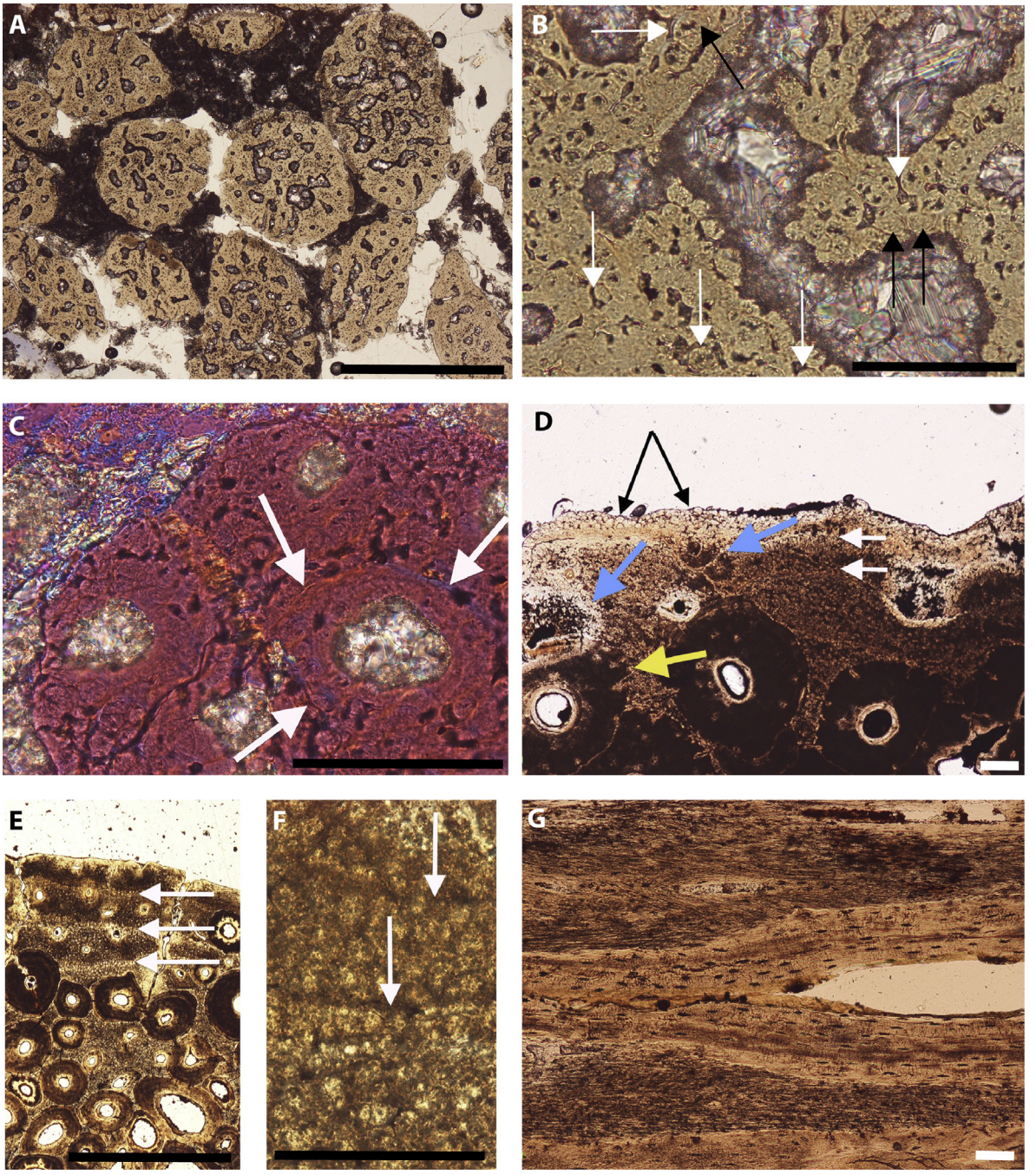

Fig. 2. (Color online.) Mineralized tendons of *Maiasaura peeblesorum* (MOR-GS400.OSS-440-4) (A–C), and mineralized tendon of *Brachylophosaurus canadensis* (MOR794-OT1-A-1) (D), (MOR 1071.Ten1-3) (E–F) and (MOR794-OT4-A-L1) (G). A. Transverse section showing a bundle of tendons from the caudal region of a small juvenile. B. Magnified view of the internal portion of a single tendon showing the individual fascicles (black arrows) and the arcuate-shaped spaces between the fascicles (white arrows). Note that the fascicles that border the vascular space show no evidence of resorption. C. Image taken in polarized light to enhance the border of what appears to be a secondary reconstruction (arrows). D. Transverse section of a mineralized tendon showing the external primary tissues near the exterior surface with secondary reconstructions toward the interior. The black arrows show the mineralized collagen fibers that would have been adjacent to the paratenon. The white arrows point out lines that have been previously referred to as lines of arrested growth of an external fundamental system. E. Magnified image showing three lines (arrows) that appear to be formed by differential orientation of fibers. F. Highly magnified image of two lines (arrows) showing that there is no evidence of a line of arrested growth. G. Longitudinal section showing a herringbone pattern of the collagen fibers within the primary tissues (upper third of the image). Scale bars in A and E are 1 mm; all other scale bars are 100 μm.

Sections removed (MOR3080.Scu1-1, MOR3080.Scu1-2) from the *Sauropelta* osteoderm (MOR 3080) were taken anterior to the keel (See Fig. SI) and nearly perpendicular to the keel's apex.

The position of the frontal and coronal sections (MOR553PN.N1-2) removed from the *Prosaurolophus* (MOR 553PN) left nasal is shown in Fig. SII.

A *Diplodocus* (MOR 592) caudal neural spine was sectioned in the transverse (MOR592.NS1-2), frontal (MOR592.NS1-L3, MOR592.NS1-L4, MOR592.NS1-L6), and sagittal (MOR592.NS1-L1) planes (Fig. SIII).

We intentionally omit discussion of pachycephalosaurid and ceratopsid skulls, previously described as having metaplastic characteristics (see Goodwin and Horner, 2004; Horner and Goodwin, 2009; Horner and Lamm, 2011), because these highly unusual tissues will be described in detail in a forthcoming study comparing and contrasting tissues formed by metaplasia and neoplasia (i.e., the transformation of a tissue *de novo*, not from pre-existing mature cells that switched their morphology and/or secretion).

3. Results

3.1. Bubo and Meleagris "ossified" tendons

The "ossified" tendons of *Bubo virginianus* and *Meleagris gallopavo* have been described regarding their similarity to "ossified" tendons of dinosaurs, and with regard to their early mineralization through the process of metaplasia (Adams and Organ, 2005; Organ and Adams, 2005). Here, we re-describe and illustrate the same tendons in order to draw attention to some additional characteristics, specifically, the rounded, off-white colored Haversian-like systems in the central region of the *Bubo* tendon (Fig. 1A–E). So as not to imply the osteoblastic origin associated with the term Haversian systems, we name the Haversian-like structures "secondary reconstructions" (SRs). The tissues that are immediately surrounding those SRs will be referred to as "peripheral" or "primary" tissues. Under low power, the SR structures appear to have borders somewhat similar to the Haversian systems (Fig. 1B) seen in cortical bone in that they possess something akin to a "cement line". In some cases, they also appear to invade or "overlap" one another (Fig. 1B white arrow). Close inspection of these SR structures (Fig. 1C, D), however, reveals that these boundaries are often indistinct (Fig. 1C, red arrows; Fig. 1D, E, all arrows) even in areas where one secondary structure meets another. In addition, a close examination shows that the primary tissues (at the exterior boundaries of the SRs) are formed of fibers organized into larger fascicles than those of the SRs (Fig. 1E, arrows show this junction). It appears that the endotenon (i.e., fine connective tissue sheath surrounding fiber bundles) of the larger fascicles undergoes destruction, or some sort of rearrangement into smaller, individual fibers within the SRs, directly around the vascular canals (Fig. 1E).

Internally, the SRs are composed of large, longitudinally oriented fibers rather than the finely fibered or plywood-like arrangement found in typical secondary osteons (Francillon-Vieillot et al., 1990). The fibers in these SRs are of similar size, and not organized in variably sized bundles (fascicles) like the fibers in the surrounding primary tendon matrix. Within the tendon, there are no cells that can be identified as osteocytes, and no evidence of canaliculi (Fig. 1C, D). The dark areas are not osteocyte lacunae but instead, are empty spaces between fiber fascicles or possibly tenocyte lacunae. The tissues immediately surrounding the vascular space (Fig. 1C, orange arrows) appear hypermineralized, as they are composed of a very dense, avascular tissue not obviously constructed of individual fibers.

In contrast to the central region, the tissues in the peripheral region of the *Bubo* tendon (darker purple) are primary, containing fascicles of variable size. These are separated from one another by spaces of differing sizes and shapes (Fig. 1C), many of which are arc-shaped (yellow arrow), suggesting they represent the location of the endotenon. At the union of the mineralized portion of the tendon and the paratenon (Fig. 1C, white arrow), the mineralization front consists of fibers, some that are unmineralized (white) and some that are mineralized (purple). The mineralization front moved in a centrifugal direction.

Just as in the tendon of *Bubo*, arc-shaped spaces are also prevalent in the *Meleagris* mineralized tendon (Fig. 1F). Unlike the *Bubo* tendon, however, the *Meleagris* tendon possesses large open vascular spaces interpreted by Organ and Adams (2005, their fig. 10A) as erosion rooms excavated by osteoclasts. We do not however see any evidence of Howship's lacunae on the channel walls, nor do we see any evidence of such boundaries on the SRs (see Fig. 1F). On the contrary, the channel walls of what appear to be newly opened vascular spaces (Fig. 1F, yellow arrows) are formed of rounded fascicles lacking any evidence of scalloped resorption. In addition, the outer boundaries of the SRs (Fig. 1F–G, white arrows) lack distinct cement line terminations, and blend or interdigitate with the primary tissues. The walls of the vascular channels within the secondary reconstructions (Fig. 1G, black arrows) seem to be

Fig. 2. (Couleur en ligne.) Tendons minéralisés de *Maiasaura peeblesorum* (MOR-GS400.OSS-440) (A–C), et tendon minéralisé de *Brachylophosaurus canadensis* (MOR794-OT1-A-1) (D), (MOR 1071.Ten1-3) (E–F) et (MOR794-OT4-A-L1) (G). A. Section transverse montrant un lot de tendons provenant de la région caudale d'un jeune. B. Agrandissement de la portion intérieure d'un tendon montrant les faisceaux individuels (flèches noires) et les espaces en forme d'arc entre ces faisceaux (flèches blanches). À noter que les faisceaux bordant les espaces vasculaires ne montrent aucune évidence de résorption. C. Image prise en lumière polarisée pour mieux visualiser la bordure d'une RS (flèches). D. Section transverse d'un tendon minéralisé montrant des tissus primaires proches de la surface externe, avec des RSs vers l'intérieur. Les flèches noires montrent les fibres de collagène minéralisées qui auraient été adjacentes au paratenon. Les flèches blanches montrent des lignes qui ont été précédemment caractérisées comme des lignes d'arrêt de croissance d'un système fondamental externe. E. Agrandissement montrant trois lignes (flèches) qui semblent être formées de fibres à orientations différentielles. F. Agrandissement plus fort de deux de ces lignes (flèches) montrant que ce ne sont pas des lignes d'arrêt de croissance. G. Section longitudinale montrant une organisation en arêtes de poisson des fibres de collagène au niveau des tissus primaires (tiers supérieur de l'image). Les barres d'échelle dans A et E représentent 1 mm, toutes les autres 100 μm.

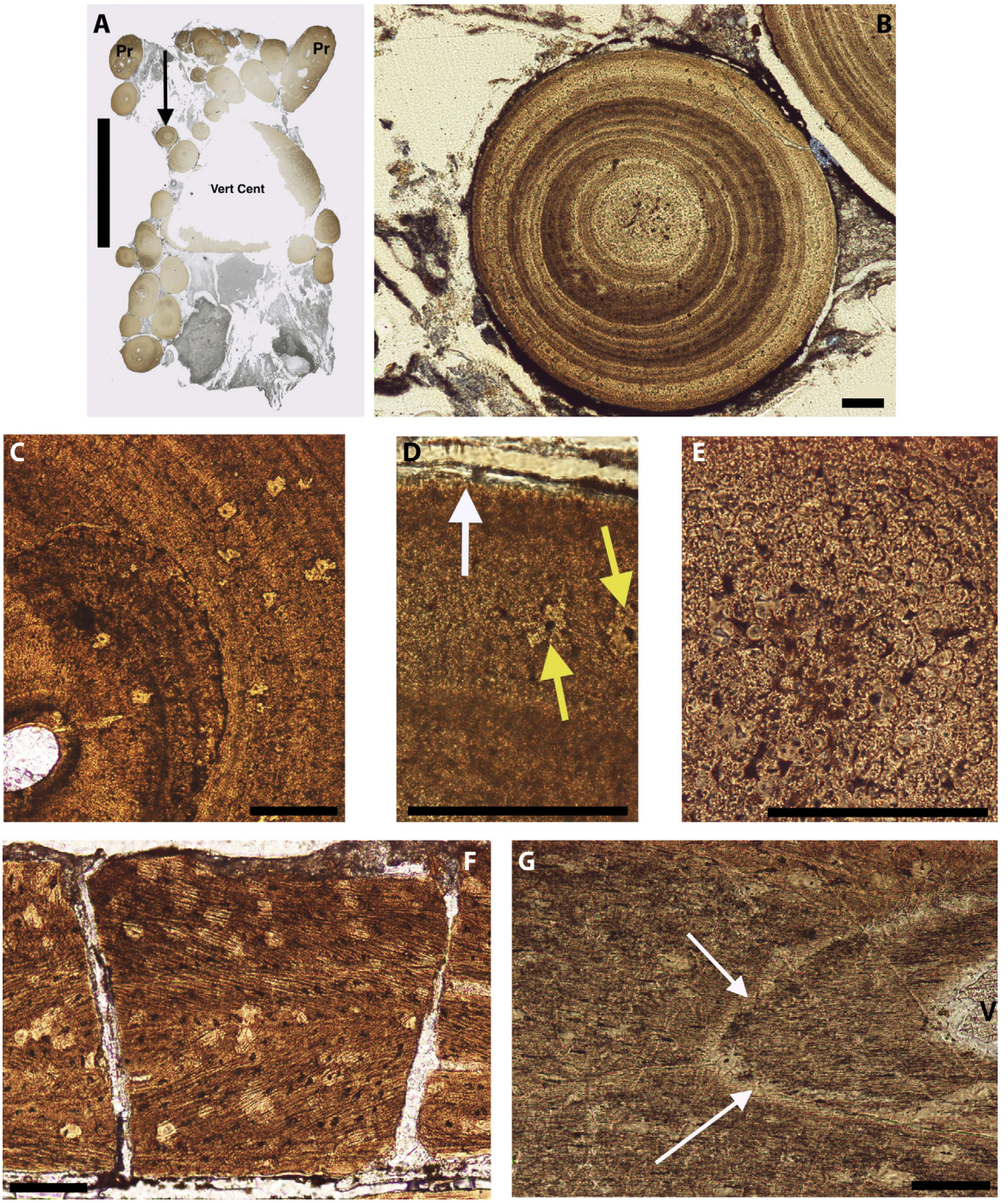

Fig. 3. (Color online.) Mineralized prezygopophyseal rods of *Deinonychus antirrhopus* (MOR747.Ten1-2) (A, B), (MOR747.Ten1-3A) (C), (MOR747.Ten1-1) (D), (MOR747.Ten1-2A) (E), (MOR747.Ten1-L2) (F, G). A. Coronal section through the caudal complex showing the orientation of the rods adjacent to a vertebral centrum (Vert Cent) and the proximal portions of its prezygopophyses (PR). The arrow points out the rod seen in B. B. A rod showing typical concentric banding. C. Magnified view of a rod showing secondary reconstructions found in sections cut near the proximal end of the prezygopophysis. Note that these secondary reconstructions are composed of dense fibers, identical in size to those in the surrounding primary tissues. Osteocyte lacunae are not evident in either the primary or secondary tissues. D. Enlarged view of the outer edge showing the individual mineralized collagen fibrils (white arrow) that would have been adjacent to a paratenon. The yellow arrows point out what appear to be small hypermineralized areas pierced by tiny vascular spaces (Note that in Fig. 3C, these same features exist in both primary and secondary tissues). E. Highly magnified center of a rod lacking a central vascular canal. Note that the entire matrix is composed of subfascicles, none of which seem to be bundled into fascicles. F. Longitudinal section (MOR747.Ten1-L2) showing typical herringbone pattern of fibers. G. Enlarged view of E, showing what appears to be a hypermineralized border between the primary tissues and a secondary reconstruction (arrows). Scale bars in A is 5 mm; all other scale bars are 100 μm.

constructed of individual fibers, apparently deposited in a centripetal direction. In longitudinal section (Fig. 1H), a herringbone pattern of the fibers is evident throughout the section.

The most salient features of these avian mineralized tendons are the highly fibrous SRs, distinct fascicles with arc-shaped boundaries, and the herringbone pattern seen in longitudinal view.

3.2. *Maiasaura and Brachylophosaurus "ossified" tendons*

The bundle of mineralized tendons (Fig. 2A–C) from the small juvenile *Maiasaura* (MOR-GS400) reveals characteristics virtually identical to those of *Meleagris*, as observed by Adams and Organ (2005). The entire tissue matrix is composed of fascicles (fiber bundles; black arrows, Fig. 2B) separated by spaces varying in size, but primarily arc-shaped (white arrows, Fig. 2B). Most of the vascular spaces resemble primary spaces in that there is no evidence that individual fiber bundles were resorbed. Instead, fascicles form the walls of these primary canals (Fig. 2B). Structures that Adams and Organ (2005) describe as first generation Haversian canals containing osteonic bone appear more similar to the SRs of the *Bubo* tendons instead, as they appear to be composed exclusively of fibers, and have indistinct outer boundaries (Fig. 2C, arrows). As mentioned earlier, the small black structures in Fig. 2B (white arrows) and C are primarily the spaces between fascicles, although some might be fibrocyte lacunae (see Adams and Organ, 2005).

The "ossified" tendons of adult *Brachylophosaurus* (MOR 794) (Fig. 2D–G) have a thin fibrous external primary matrix that looks very similar to the primary tissues of the *Bubo* and *Maiasaura* tendons. Mineralized fibers form the periphery of the tendon (Fig. 2D, black arrows), identical to the peripheral mineralized portion of the *Bubo* tendon. Parallel lines near the tendon surface (Fig. 2D–F, white arrows) do not look like distinct arrested growth lines (LAGs), and we hypothesize that they are rather zones of varying fiber density and orientation change as revealed by color differences (Fig. 2F, arrows).

Internal to the primary tissues are dark, rounded SR features composed of dense fibers similar to the white colored SRs seen in the *Bubo* tendon (Fig. 1). The SRs nearest the periphery of the tendon contain the greatest density of fibers, and those found more centripetally have fewer fibers and more closely resemble true secondary osteons (Fig. 2D–E).

Some vascular canals within the primary tissues of this "ossified" tendon are surrounded by unusual, discolored tissue (Fig. 2D, blue arrows). The right blue arrow (Fig. 2D) indicates what appears to be a SR feature missing its upper half, while the lower portion seems to "overlap" or invade another SR feature. The left blue arrow points to a concentric off-white area around a vascular space that appears to invade or "overlap" an adjacent SR; this SR in turn invades yet another adjacent SR. In addition, the primary tissues interdigitate with SR tissues at the yellow arrow in Fig. 2D.

In longitudinal view (Fig. 2G), the *Brachylophosaurus* mineralized tendon reveals its highly fibrous primary matrix in herringbone arrangement, penetrated by a few vascular canals. The herringbone pattern, composed of fibers organized in juxtaposing directions, gives the appearance of the LAGs seen in transverse section (e.g. Fig. 2E). Centrally located in Fig. 2G is a longitudinally oriented Haversian-like system containing osteocyte lacunae with canaliculi.

3.3. *Deinonychus tail rods*

Deinonychus, like other dromaeosaurid dinosaurs, had elongated rod-like prezygopophyseal processes and chevrons (Fig. 3A, B and see Ostrom, 1969). Organ and Adams (2005) disagreed with Ostrom's (1969) hypothesis that the tail rods developed within tendon sheaths that functioned similar to a periosteum. In the view of Organ and Adams (2005), tail rods did not undergo metaplasia, but rather accumulated small amounts of circumferential apposition as elongated processes of the vertebrae, and therefore likely possessed a true periosteum. Moreover, they identified tail rods of *Deinonychus* as more vascular near the vertebral body, and becoming devoid of vascularity distally. While we confirm the lack of obvious distal vascularity, the actual composition of the tail rods is inconsistent with bone deposited within a periosteum. Rather, the tail rods are composed exclusively of longitudinally oriented fibers (Fig. 3B–F), including within most SRs (Fig. 3C). A close inspection of the exterior surface (Fig. 3D, arrow) reveals fibrils, indicating a paratenon, rather than a periosteum, was once present. Circumferential banding of light and dark zones (Fig. 3B), characteristic of dromaeosaurid tail rods, is the product of differential orientation and density of the fibers, resulting from the herringbone pattern seen in longitudinal view (Fig. 3F). The lightest colored zones, including the central region of the tail rod and a concentric ring near the periphery, are composed of loosely organized fibrils with relatively large variably shaped spaces between fascicles (Fig. 3B, E).

Fig. 3. (Couleur en ligne.) Apophyses allongées de vertèbres caudales minéralisées de *Deinonychus antirrhopus* (MOR747.Ten1-2) (A, B), (MOR747.Ten1-3A) (C), (MOR747.Ten1-1) (D), (MOR747.Ten1-2A) (E), (MOR747.Ten1-L2) (F, G). A. Section coronale du complexe caudal montrant l'orientation des tiges adjacentes au corps vertébral (Vert Cent), ainsi que les parties proximales des prézygopophyses (PR). La flèche montre la tige observée en B. B. Tige montrant des bandes concentriques. C. Agrandissement d'une tige montrant les RSs des sections proches des parties proximales de prézygapophyses. Notez que ces RS sont composées de fibres identiques à celles qui entourent les tissus primaires. Ces tissus ne montrent aucune lacune ostéocytaire. D. Agrandissement de la limite extérieure montrant des fibres minéralisées de collagène (flèche blanche) qui auraient été adjacentes à un paratenon. Les flèches jaunes indiquent des aires apparemment hyperminéralisées, percées par de petits espaces vasculaires (à noter que ces mêmes caractéristiques peuvent être observées dans les tissus primaires et secondaires de la figure C). E. Agrandissement très fort du centre d'une tige dépourvue de canal vasculaire. À noter que toute la matrice est composée de fibres, et qu'aucune d'elles ne semble être organisée en plus grand faisceau. F. Section longitudinale (MOR747.Ten1-L2) montrant une organisation en arêtes de poisson. G. Agrandissement de E, montrant ce qui apparaît être une bordure hyperminéralisée entre les tissus primaires et des RSs (flèches). La barre d'échelle dans A représente 5 mm, toutes les autres 100 μm.

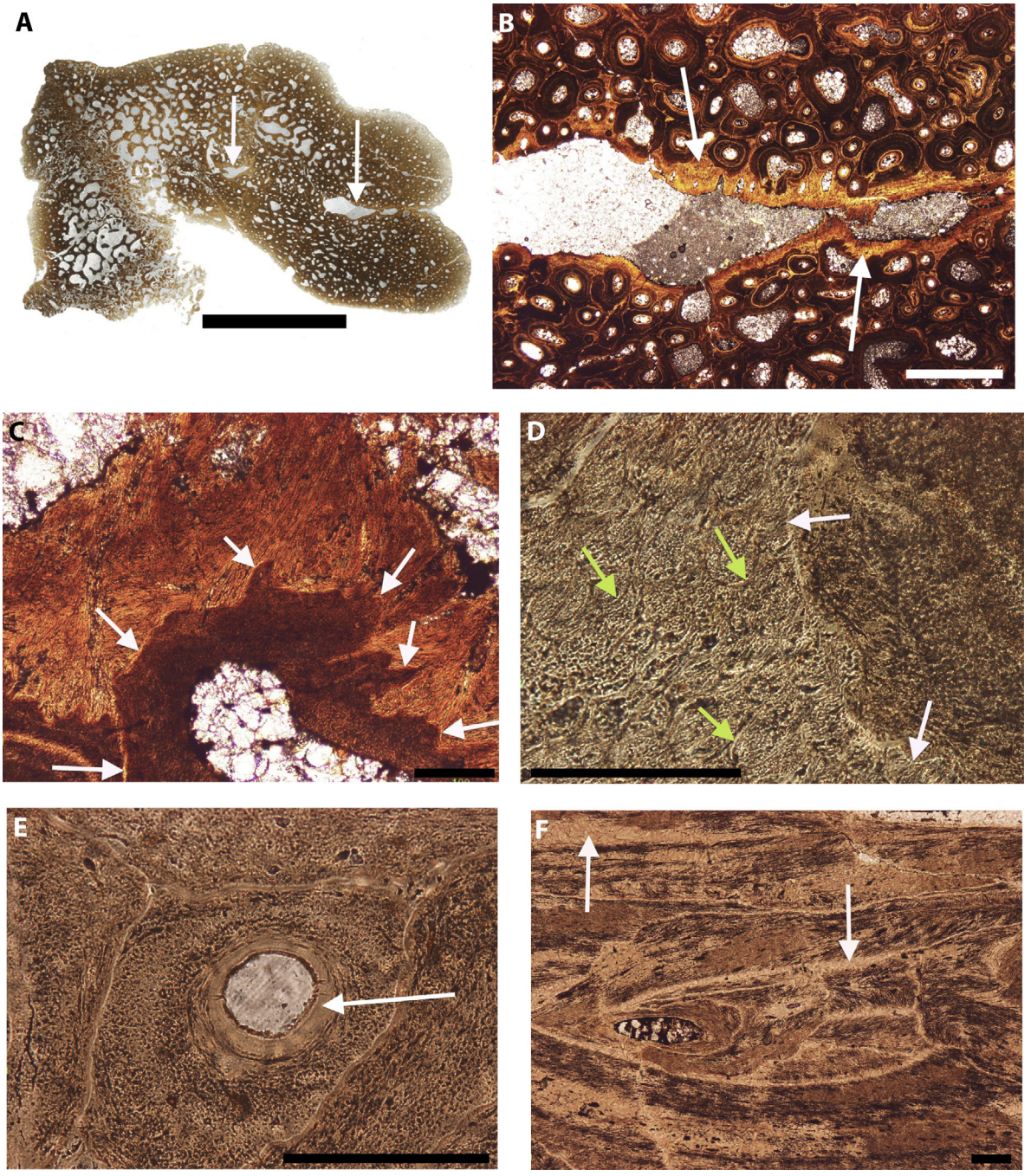

Fig. 4. (Color online.) Sections through the lateral side of a cf. *Euoplocephalus* tail club "handle" (MOR.H.2010-09.TC1-2) (A–E), (MOR.H.2010-9.TC1-L2) (F). A. Coronal section showing two spaces (arrows) between what are thought to be two tendon-like structures. It is within these spaces that primary tissues are located. Secondary reconstructions reach the external surfaces of the entire specimen. B. Magnified image of the space showing the thin veneer of primary tissues (arrows). C. Enlarged view of B showing the junction (arrows) between the primary tissue (light orange) and darker secondary reconstructions (dark orange). Note the extremely irregular border of the secondary reconstruction, and the lack of osteocytes lacunae. D. Magnified view of primary tissues composed of fascicles. Note the arc-shaped boundaries of the fascicles (green arrows), and the border of a secondary reconstruction (white arrows) clearly composed of smaller fiber bundles. E. Highly magnified view showing vascular canal of a secondary reconstruction thought to have a border of hypermineralized tissue (arrow). F. Longitudinal section showing the typical herringbone pattern and hypermineralized borders (arrows). Scale bar in A is 1 cm and in B is 1 mm; all other scale bars are 100 μm.

Crescent shaped spaces can be seen around the fascicles (Fig. 3E).

In regions proximal to the vertebrae where vascularity exists, the majority of vascular space is surrounded by SR tissues that are composed of dense fibers (Fig. 3C, F). A zone of apparent hypermineralized, avascular and acellular tissue separates the primary matrix from the SR (Fig. 3G, arrows).

3.4. Cf. Euoplocephalus sp. "tail club handle"

A fragmentary specimen originating from the lateral surface of a *Euoplocephalus* (MOR 2010-09) tail "handle" reveals rounded tendon-like structures (Fig. 4A–F). Interestingly, there is no evidence of primary tissue on any exterior surface, but it is present more internally between the tendon-like structures (Fig. 4A, B, arrows). At higher magnification, this internal region is seen to consist of densely fibrous primary tissues (Fig. 4C) and SRs with extremely irregular borders (Fig. 4C, white arrows). In some regions, the fiber bundles making up the primary tissues are oriented perpendicular to the plane of section, and clearly show the round endotenon walls (Fig. 4D, green arrows). In some of the SR structures, the tissues adjacent to the vascular spaces appear to be hypermineralized (Fig. 4E). A longitudinal section through a region of multigenerational SRs (Fig. 4F) reveals dense structural fibers generally arranged in herringbone patterns separated by hypermineralized zones (arrows).

3.5. Sauropelta osteoderm

Scheyer and Sander (2004) published an excellent review of ankylosaur osteoderm histology with which we agree, and we therefore describe only a single nodosaur osteoderm to highlight particular characteristics relevant to our study. This *Sauropelta* (MOR 3080) osteoderm has three distinct regions, the dorsal compact zone, the middle trabecular zone, and the ventral compact zone (respectively, DZ, MZ and VZ in Fig. 5A). All of the primary tissues are located in a thin veneer adjacent to the dorsal surface, and on low magnification, these primary tissues appear to be laminated (Fig. 5B, arrow). Upon closer inspection, however the layers are simply parallel bands of fibers with different orientations and therefore different coloration (Fig. 5C). Small dark structures that initially resemble osteocyte lacunae are instead mostly arc-shaped spaces bordering fascicles (arrows, Fig. 5D), although some may possibly be the lacunae of fibrocytes or tenocytes. Higher magnification reveals a group of fiber bundles oriented perpendicular to the plane of the section (Fig. 5E). The only features observable here are fibers and the spaces between them. Under high magnification, arcuate spaces within the outer tissues including those on the exterior surface (arrows, Fig. 5F) reveal densely packed fascicles.

The middle of the specimen is cancellous (Fig. 5A) and composed of secondarily remodeled bony trabeculae. The ventral zone is composed of a more compacted secondarily reworked tissue that lacks many fibers (Fig. 5G).

3.6. Prosaurolophus nasal

A frontal section through the nasal of the ornithopod *Prosaurolophus* (MOR 553 PN; Fig. 6A–F) reveals dense Haversian-like tissues reaching all borders, except the dorsal surface where a thin veneer of primary tissue is preserved (Fig. 6B, white arrows). A few islands of primary tissue exist between deeper SRs (Fig. 6B, yellow arrow). Moderate magnification (Fig. 6C) reveals primary tissues composed of circular bundles of dense fibrils and fascicles oriented in a rostral-caudal direction. Structures resembling osteocyte lacunae are generally spaces between fascicles (Fig. 6C and arrows in Fig. 6D) and many of these spaces are arcuate in shape (Fig. 6C–E). Some vascular spaces seem to have hypermineralized tissues surrounding the vascular canals (Fig. 6D). The SRs embedded within and directly adjacent to the primary tissues have highly irregular borders (see Fig. 6E, arrow as example) and are densely fibrous. The SRs in the central region of the section have irregular borders, and contain varying amounts of fibrous tissues (Fig. 6F). In longitudinal (rostral-caudal) view (Fig. 6G), the fibers in the primary tissues have either a herringbone or parallel orientation. The parallel fibered regions have a banded appearance that is created by differential orientation of fibers.

3.7. Diplodocus Caudal Neural Spine

Reid (1996) called attention to the "readily demonstrable" metaplastic tissues found on interspinous ligament scars in saurischian dinosaurs. These tissues are clearly seen in the sections of the *Diplodocus* (MOR 592) neural spines forming a thin veneer on both the anterior and posterior rugose surfaces (Fig. 7A, arrows). In polarized light (Fig. 7B), the primary tissues contrast with the dark SRs. The primary tissues are oriented perpendicular to the rostral and caudal faces of the neural spine (Fig. 7C), and in line with the collagenous fiber orientation that would have existed within the original interspinous ligament. The primary tissues are extremely dense and are therefore likely hypermineralized calcified fibrocartilage. Globular structures, scattered through the primary tissues (See Fig. 7D,

Fig. 4. (Couleur en ligne.) Sections au travers du côté latéral de la base de la massue de la queue d'*Euoplocephalus* (MOR.H.2010-09.TC1-2) (A–E), (MOR.H.2010-9.TC1-L2) (F). A. Section coronale montrant deux espaces (flèches) entre des structures ressemblant à des tendons. Les tissus primaires sont présents à l'intérieur de ces espaces. Les RSs atteignent les surfaces externes de ce spécimen. B. Agrandissement de l'espace montrant une veine très fine de tissus primaires (flèches). Agrandissement de B montrant la jonction (flèches) entre le tissu primaire (orange clair) et les RSs (orange foncé). À noter que les bordures des RSs sont extrêmement irrégulières, et l'absence de lacunes ostéocytaires. D. Agrandissement des tissus primaires composés de faisceaux. À noter les limites en forme d'arc entre les faisceaux (flèches vertes), et la limite d'une RS (flèche blanche), clairement composée de faisceaux plus petits. E. Agrandissement très fort montrant un canal vasculaire de RS, bordé d'un tissu apparemment hyperminéralisé (flèche). F. Section longitudinale montrant l'arrangement en arêtes de poisson et les bords hyperminéralisés (flèches). La barre d'échelle dans A et B représentent 1 cm et 1 mm respectivement ; toutes les autres représentent 100 μm.

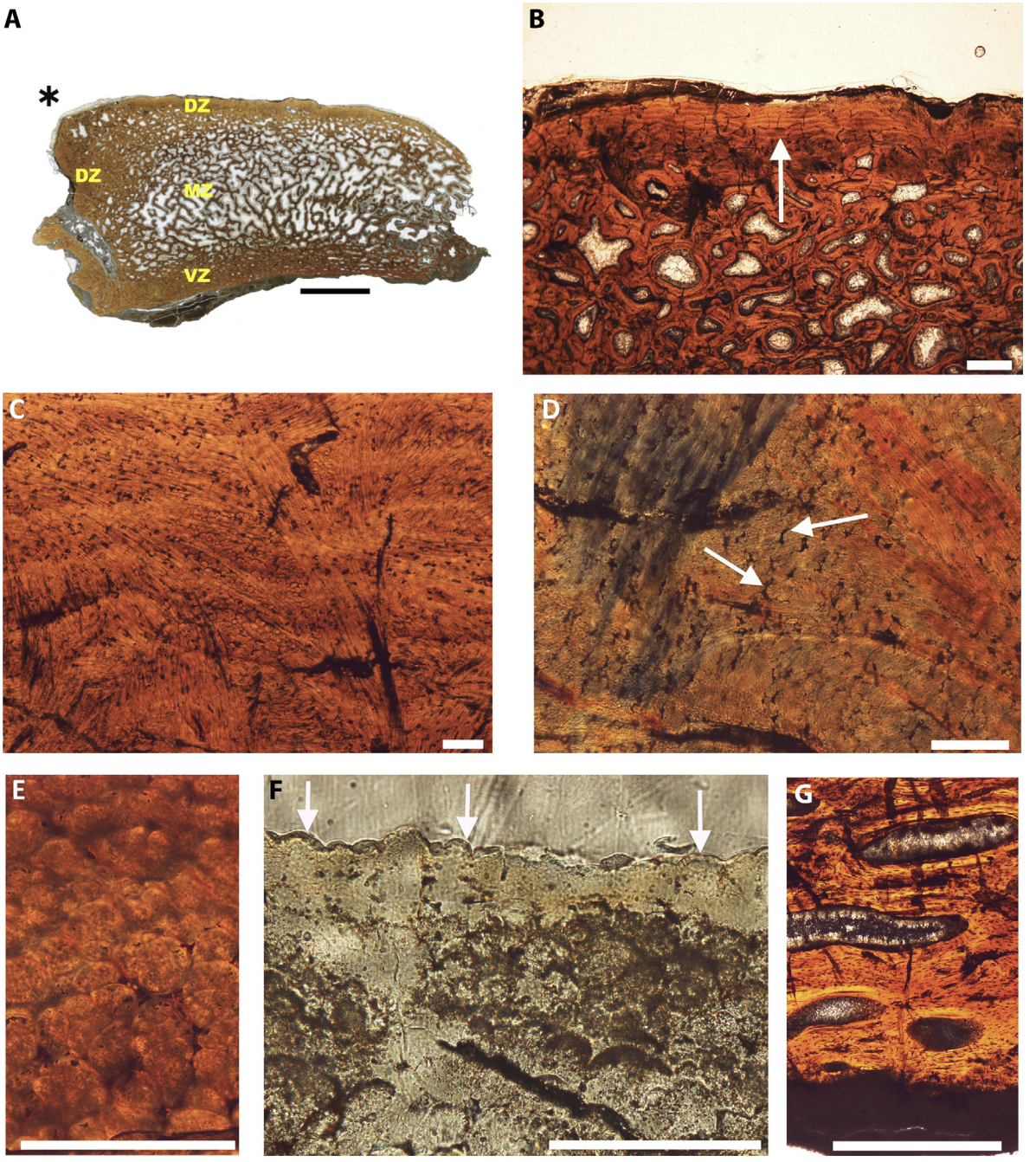

Fig. 5. (Color online.) Sections through a cf. *Sauropelta* osteoderm (MOR3080.Scu1-2) (A–D, F). (MOR3080.Scu1-1) (E). A. Three vertical zones, the dorsal zone (DZ), middle zone (MZ) and ventral zone (VZ). Star is a reference point to orient the slice with the original element (see Supp. Info, Fig. SI). Scale bar is 1 cm. B. Magnified image showing banding in the DZ (arrow). C. Magnified bands revealing that they are coloration differences, and that the collagen fibers are running in many differing directions. D. Highly magnified area showing that most of the dark structures represent arc-shaped spaces between fascicles. E, MOR3080.Scu1-1 showing extremely magnified fasciles with encased fibrils. F. Extremely magnified dorsal surface showing rounded fasciles bordering the surface. G. Image showing that the VZ is composed of typical secondary trabecular bone. Scale bar in A is 1 cm, in B and G is 1 mm; all other scale bars are 100 μm.

Fig. 5. (Couleur en ligne.) Sections dans un ostéoderme de *Sauropelta* sp. (MOR3080.Scu1-2) (A–D, F). (MOR3080.Scu1-1) (E). A. Image montrant trois zones verticales, la zone dorsale (DZ), la zone intermédiaire (MZ) et la zone ventrale (VZ). L'astérisque est un point de référence pour orienter l'image (voir les informations supplémentaires,SI). La barre d'échelle représente 1 cm. B. Agrandissement montrant des bandes dans la DZ (flèche). C. Agrandissement de ces bandes montrant leurs colorations différentes et l'orientation différentielle des fibres de collagène. D. Agrandissement très fort montrant que les structures foncées représentent des espaces en forme d'arc entre les faisceaux fibreux. E, MOR3080.Scu1-1, montrant ces faisceaux et leurs fibres à fort grossissement. F. Grossissement extrêmement fort au niveau de la surface dorsale, montrant des faisceaux ronds à cet endroit. G. Image montrant que la VZ est composée d'os secondaire trabéculaire typique. La barre d'échelle dans A représente 1 cm, dans B et G, 1 mm ; toutes les autres barres représentent 100 μm.

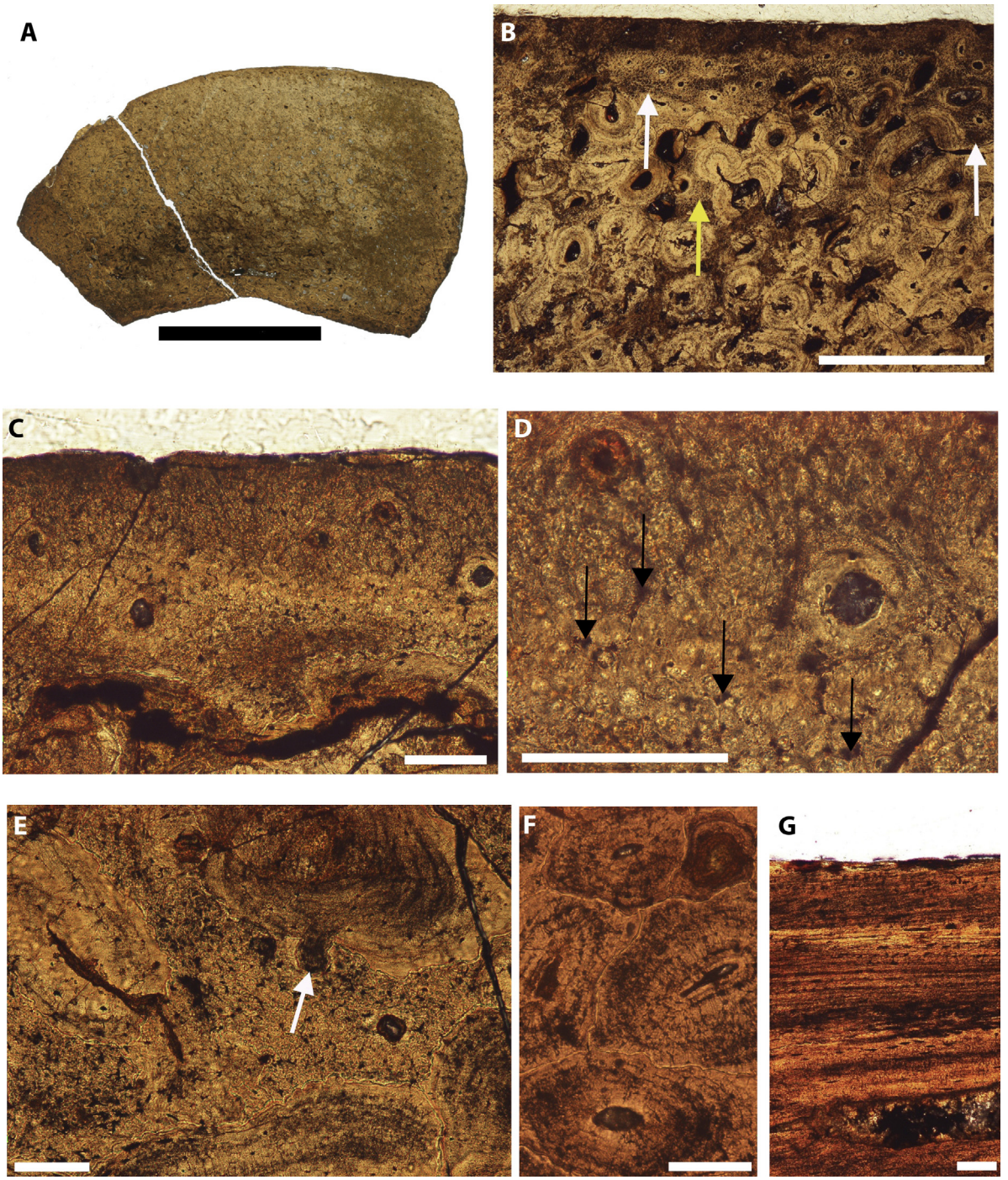

Fig. 6. (Color online.) Sections from the nasal of *Prosaurolophus* (MOR553PN.N1-2) (A, C–F), (MOR553PN.N1-1) (B), (MOR553PN.N1-L2) (G) (See Supp. Info. Fig. SII for section orientation). A. Whole section with the medial junction to the right. B. Image from the dorsal surface with white arrows showing the inner boundary of the thin veneer of primary tissue. The yellow arrow points out an island of primary tissue. C. Magnified view of the primary tissues at the dorsal surface. Note that the primary tissues are bundles of fibers oriented perpendicular to the slide, and that each fascicle is bound by arc-shaped spaces. Densely fibered secondary reconstructions are seen at the bottom of the image. D. Highly magnified view of the fascicles, the arc-shaped spaces (black arrows) and a couple vascular spaces with what appears to be hypermineralized borders. E. Densely fibered secondary reconstructions with highly irregular borders. The white arrow points out a protruded part of the reconstruction. F. Secondary reconstructions found deeper in the nasal show less fiber and more characteristics of typical Haversian systems. G. Rostral-caudal section showing the longitudinal orientation of the primary fibers and the longitudinally elongated secondary reconstruction (lower half of image). Scale bar in A is 1 cm, in B is 1 mm; all other scale bars are 100 μm.

arrow), are likely some crystals of hydroxyapatite forming this mineralized fibrocartilage. The hypermineralized tissues are interdigitated with a zone of highly fibrous SRs. Although rare, there are a few primary vascular spaces (Fig. 7B, yellow arrow; Fig. 7D, arrow). These open spaces are not typical erosion rooms as there is no evidence of osteoclastic resorption in the classic sense with Howship's lacunae. Rather, the spaces are lined with the globular shaped lacunae. In rostral-caudal view, the densely fibrous SRs are delineated from the hypermineralized matrix by different fiber orientation (Fig. 7E, F, arrows). Internal to the thin veneer of calcified tissue from either the rostral or caudal faces the SRs are densely fibrous and possess highly irregular borders (Fig. 7G). Most appear as if they were stretched in the rostral-caudal direction (dark structures in Fig. 7B).

In frontal section (Fig. 8A–G), the calcified tissues (Fig. 8A, B, blue arrows) are interspersed with variously shaped SRs. Most of the SRs have a rounded shape indicative of longitudinal vascular channels in a rostral-caudal orientation, but some, particularly in the central region of the specimen, are oriented dorso-ventrally. Interestingly, erosion rooms with scalloped walls (Howship's lacunae) are absent in both primary and secondary tissues.

Highly magnified (Fig. 8C), primary tissues appear largely composed of a non-fibrous hypermineralized matrix with tiny, mostly round tunnels that probably enclosed unmineralized collagen fibrils. Also within the primary tissues are a fair number of primary vascular canal – like openings with varying concentric coloration zones surrounding them (Fig. 8B, D, E, G). The simplest type consists of concentric coloration rings (arrows) arranged around an unorganized vascular-like space (Fig. 8D). The calcified matrix appears to have been breaking apart in the central region, although there is no evidence of osteoclastic resorption. The innermost ring surrounding the vascular space is darker (yellow arrows) than the ring farthest away (green arrows). Lighter colored regions separate the dark rings. Another similar looking structure (Fig. 8E) has a more organized vascular opening, but similar to the previous structure lacks evidence of osteoclastic resorption, and possesses a much darker (brown) region adjacent to the vascular opening (yellow arrows). The outer coloration ring (green arrows) is a lighter brown color. A magnified view of the region extending out from the vascular space shows much of the discoloration results from many of the tiny round tunnels containing black colored infillings (Fig. 8F, white line). Beyond this darker colored region, most of the tiny rounded tunnels are empty (yellow line). The dark in-filled tunnels most likely contain fibrils that have undergone mineralization. A third structure (Fig. 8G) has a much wider dark zone, and looks very similar to other nearby SRs, except that it lacks a distinct outer boundary. The inner rim around the edge of the vascular opening appears to consist of a more evenly distributed and denser mineralized tissue.

Structures we refer to as mature, fibrous SRs (Fig. 9A) have a central vascular canal, and an outer series of alternating light and dark concentric rings, with a fairly distinct exterior boundary. The exterior boundary does not however, reveal any evidence of being initially formed by osteoclastic resorption as it lacks evidence of Howship's lacunae. The edges of these SRs seem to interdigitate with the mineralized primary matrix (just like what is shown in Fig. 1C–E). Only where these SRs meet and invade one another do there appear to be rounded scallop-like edges (Fig. 9A, arrows). Highly magnified, the light and dark concentric rings of the SRs (Fig. 9B) are a series of coloration changes afforded apparently by differential orientation of the dense fiber network, or possibly represent mineralization fronts. While it is possible that the alternating color bands are diagenetic in origin, the completed structures are identical to the SRs from all of the specimens described in this study.

Some SRs apparently underwent partial destruction as their concentric rings and overall shapes are disrupted or distorted (Fig. 9C–E, arrows). Interestingly, the disrupted or distorted edges only exist within the primary matrix, and not where they intersect other SRs (See Fig. 9E). Fig. 9F reveals an instance where a simple vascular space with outer concentric rings has invaded a mature SR (arrow). At this point, there is no distinct line between the two features other than the dense fibers of the structure on the right having been either deformed or destroyed by the inclusion of the structure on the left.

4. Discussion

As mentioned in the introduction, metaplasia is the permanent transformation of a cell type into another, which in turn leads to a change in tissue type. In the present study, we hypothesize that a number of dinosaurian mineralized tissues formed through metaplastic transformation, rather than by periosteal and intramembranous ossification. Recently, Vickaryous and Hall (2008) found that the osteoderms of *Alligator mississippiensis*, a member of the extant phylogenetic bracket of the Dinosauria, form through metaplasia. These osteoderms were described as forming without any periosteum and from the direct mineralization of dense fibrous connective tissues. Most likely, a population of fibroblast-like cells transform into osteoblast-like cells, but this could only be determined by *in situ* hybridization and immuno-histochemistry in some

Fig. 6. (Couleur en ligne.) Sections de l'os nasal de *Prosaurolophus* (MOR553PN.N1-2) (A, C–F), (MOR553PN.N1-1) (B), (MOR553PN.N1-L2) (G) (voir les informations supplémentaires, Fig. SII pour comprendre l'orientation). A. Section entière avec la jonction médiale à droite. B. Image provenant de la surface dorsale avec les flèches blanches indiquant la limite interne de la veine fine de tissu primaire. Les flèches jaunes montrent un îlot de tissu primaire. C. Vue agrandie des tissus primaires de la surface dorsale. À noter que les tissus primaires sont des faisceaux fibreux orientés perpendiculairement à la section, et que chaque faisceau est séparé d'un autre par un espace arqué. Des RSs très fibreuses peuvent être observées au bas de l'image. D. Vue très agrandie des faisceaux, des espaces arqués (flèches noires) et de deux espaces vasculaires avec leurs bordures apparemment minéralisées. E. RSs très densément fibreuses, avec bordures irrégulières. La flèche blanche montre une partie qui dépasse de la reconstruction. F. RSs localisées plus profondément dans l'os nasal et montrant moins de fibres et plus de caractéristiques typiques des systèmes haversiens. G. Section rostro-caudale montrant l'orientation longitudinale des fibres primaires et une RS allongée (bas de l'image). Les barres d'échelle dans A et B représentent 1 cm et 1 mm respectivement, toutes les autres représentent 100 μm.

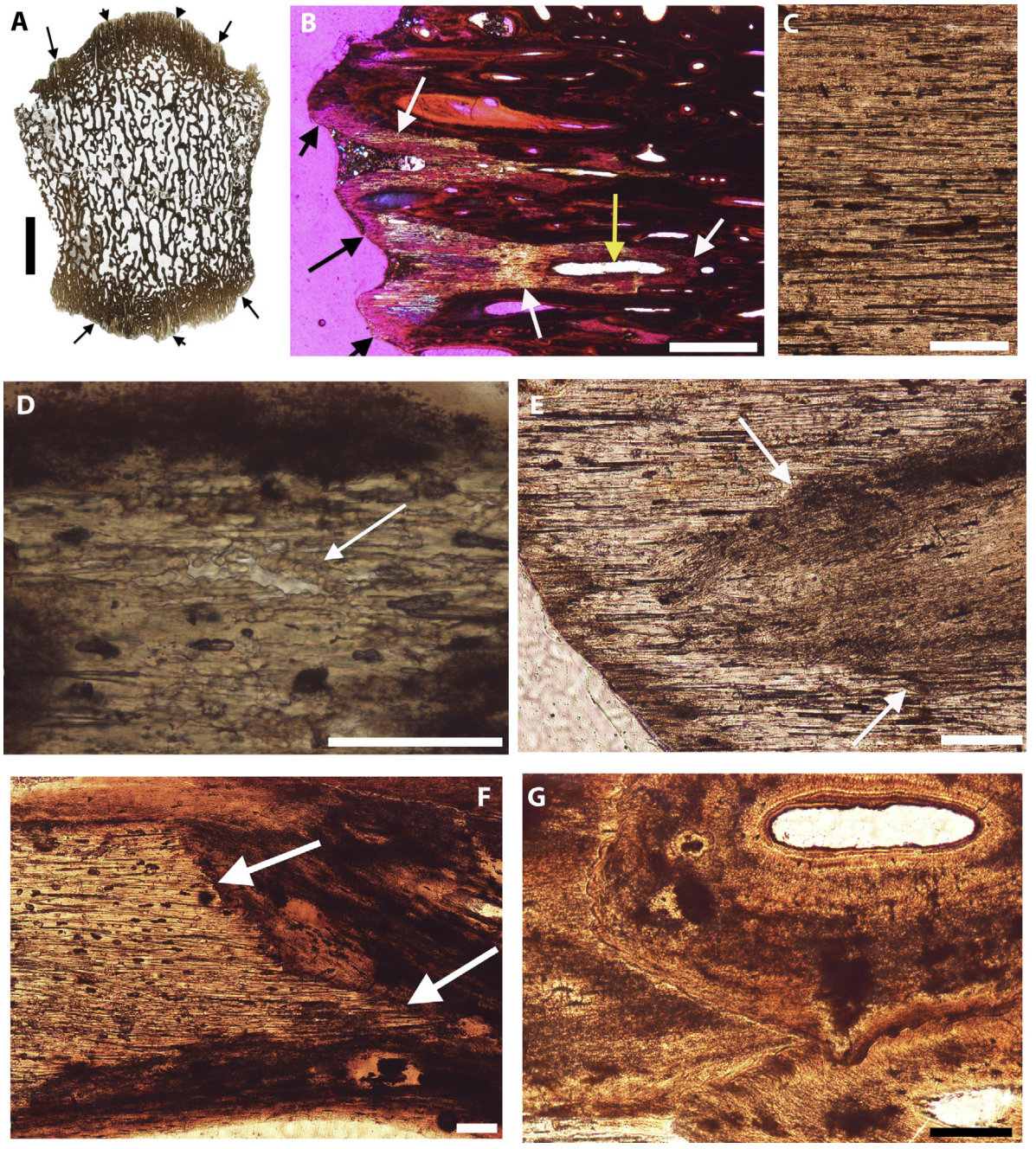

Fig. 7. (Color online.) Transverse and sagittal sections through the caudal neural spine of a young *Diplodocus* (MOR592.NS1-2) (A–E, G), (MOR592.NS1-L1) (F) (see Suppl. Info.,SIII, for slide orientation). A. Whole slide showing a thin veneer of metaplastic (hypermineralized calcified fibrocartilage) tissue (arrows). B. Rostral surface in polarized light showing the metaplastic tissues (white arrows) and an open space (yellow arrow) within the primary tissues. The black arrows point out the "tide mark" that would have formed the boundary between the uncalcified and hypermineralized calcified fibrocartilage. C. Image showing the very straight orientation of the hypermineralized calcified fibrocartilage. The black lines are likely in-filled tiny round holes (see Fig. 8F). D. Globular structures (arrow) thought to be mineralized fibrocartilage. E. A highly fibrous secondary reconstruction. Note the elongate cell lacunae in the mid portion of the reconstruction. F. View of the mineralized fibrocartilage and secondary reconstruction boundary (arrows) showing the union to be highly irregular and not scalloped. G. Highly fibrous secondary reconstructions located deeper into the neural spine. Scale bar in A is 1 cm, in B is 1 mm; all other scale bars are 100 μm.

extant species (Matthew Vickaryous, *personal communication*). This is beyond the scope of this paper and having shared our assumption, we will only focus on histological structures and the processes that might have followed this cellular metaplasia.

There is a number of striking histological similarities between the mineralized tendons of the two extant birds (avian theropod dinosaurs) and the various skeletal elements from the non-avian dinosaur taxa described herein. As detailed in their extensive paper on hadrosaurian "ossified" tendons, Adams and Organ (2005) determined that the epaxial tendons follow a very similar ontogenetic sequence as those of bird mineralized tendons, except in the final stages of mineralization. Adams and Organ (2005) propose that following the similar initial mineralization patterns of bird tendons, the hadrosaurian tendons underwent a transformation from metaplastic mineralization to periosteal mineralization. This transformation, they suggest, occurred when hadrosaurs reached skeletal maturity and began to form an external fundamental system (EFS). We did not find any evidence to contradict this hypothesis, but do emphasize that the lines we found in the "ossified" tendons of the *Brachylophosaurus* (MOR 794) definitely do not present characteristics of LAGs, but instead mineralization fronts or some other line formed from differential fibril orientation. In addition, the *Brachylophosaurus* specimen from which the tendons were derived had clearly not reached skeletal maturity as an EFS was not found in any of its skeletal elements (*JRH, personal observation*). We agree that the initial process of tendon mineralization in the two hadrosaurs discussed here was very similar to what is observed in birds; with the exception that mineralization occurred ontogenetically much earlier in non-avian dinosaurs, as the high degree of vascularization seen in juvenile hadrosaur mineralized tendons (Fig. 2A) is indicative of early mineralization (Landis et al., 2002). However, the mineralization is more likely calcification rather than true ossification, a distinction we discuss in further detail below. Additionally, we found (during our initial survey of dinosaur tissues) that not all "ossified" tendons have identical histologies (see Organ and Adams, 2005), even among the hadrosaurs. (e.g., Moodie, 1928). The *Brachylophosaurus* specimens were the only specimens with histologies comparable to those of the avian tendons. A much more detailed study is necessary to determine if the "ossified" tendons of dinosaurs formed through differing processes.

With the exception of the thin enthesis tissues observed in the vertebrae of the sauropod, the primary tissues and adjacent SRs of all other dinosaur elements described herein are fairly consistent in their organization. Primary tissues are composed of variously oriented dense fibrils or fascicles separated by arc-shaped spaces, and the adjacent SRs are extremely fibrous. There is no evidence of either the primary tissues or initial SRs having been formed by osteoblasts nor is there any evidence of osteocytes (discussion concerning the osteocytes of Fig. 2G will follow). Instead, all of these tissues exhibit characteristics very similar or identical to the ossified tendons of the avian taxa, and mineralized through a process of metaplasia.

Most significant is the fact that both primary and secondary tissues within all of the samples are densely fibrous (excluding the primary tissues of the sauropod enthesis), calling particular attention to SR formation. As first discussed by Scheyer and Sander (2004), fibrous SRs are difficult to interpret with regard to their development. Scheyer and Sander (2004) suggested two possibilities: the fibers were not resorbed by the osteoclasts that removed primary tissues, or alternatively, new fibers were incorporated during the centripetal deposition of the secondary tissues. We think there is a third possibility: that the reconstructing cells were not the standard osteoclasts and osteoblasts normally responsible for the formation of secondary osteons, and instead, the process is wholly different than the typical resorption and subsequent deposition processes of ossified bone. The highly irregular borders of the first generation SRs suggest that alteration of the fibrous primary tissues occurred by cells other than typical osteoclasts. Destruction of the fibrous matrix and formation of the initial vascular spaces were more likely accomplished by some type of enzymatic lysis. In such a scenario, it is plausible that remodeling was accomplished by fibrocytes (see Ten Cate, 1972), fibroblasts, or an unknown macrophage (see Fallon et al., 1983; Witten and Villwock, 1997). The SRs in the *Bubo* (MOR 2001-10R) ossified tendon have exactly the same architecture as the SRs of the non-avian dinosaurs, and it is therefore likely that identical processes were responsible.

In his detailed description of mineralization in chicken tendons, Abdalla (1979) noted the irregular shapes of initial Haversian systems, but did not mention any particular differences in composition between the primary and secondary tissues. Interestingly, as stated by Abdalla (1979), with succeeding "Haversian" generations, the walls became less irregular and more concentric, just as observed within the internally reworked regions of the non-avian dinosaur elements described here, such as seen in Fig. 6F.

Regardless of the processes that altered the primary tissues and created the irregular "cement lines" or the cell type responsible for secondary organization of the dense fibers, the actual morphology of these SRs is peculiar. As illustrated in Figs. 8 and 9, it appears that the secondary structures are not at all the result of osteoclastic resorption and osteoblastic deposition, but rather changes in the overall consistency of the mineralized fibrocartilage. Fig. 8D

Fig. 7. (Couleur en ligne.) Sections transverses et sagittales d'une épine neurale caudale d'un jeune *Diplodocus* (MOR592.NS1-2) (A–E, G), (MOR592.NS1-L1) (F) (voir les informations supplémentaires, Fig. SIII pour comprendre l'orientation). A. Section entière montrant une veine fine de tissu métaplastique (fibrocartilage hyperminéralisé, flèches). B. Surface rostrale en lumière polarisée montrant les tissus métaplastiques (flèches blanches) et un espace ouvert (flèche jaune) avec des tissus primaires. Les flèches noires indiquent une zone formant la limite entre le fibrocartilage non calcifié et calcifié. C. Image montrant l'orientation très droite du fibrocartilage hyperminéralisé. Les lignes noires sont vraisemblablement des espaces remplis de minéraux (voir Fig. 8F). D. Structures globulaires (flèche) étant apparemment du fibrocartilage minéralisé. E. SR très fibreuse. À noter les lacunes cellulaires allongées au milieu de la zone de reconstruction. F. Limite entre le fibrocartilage et une RS (flèche) montrant une jonction très irrégulière. G. RS très fibreuse localisée plus profondément dans l'épine neurale. Les barres d'échelle dans A et B représentent 1 cm et 1 mm respectivement, toutes les autres représentent 100 μm.

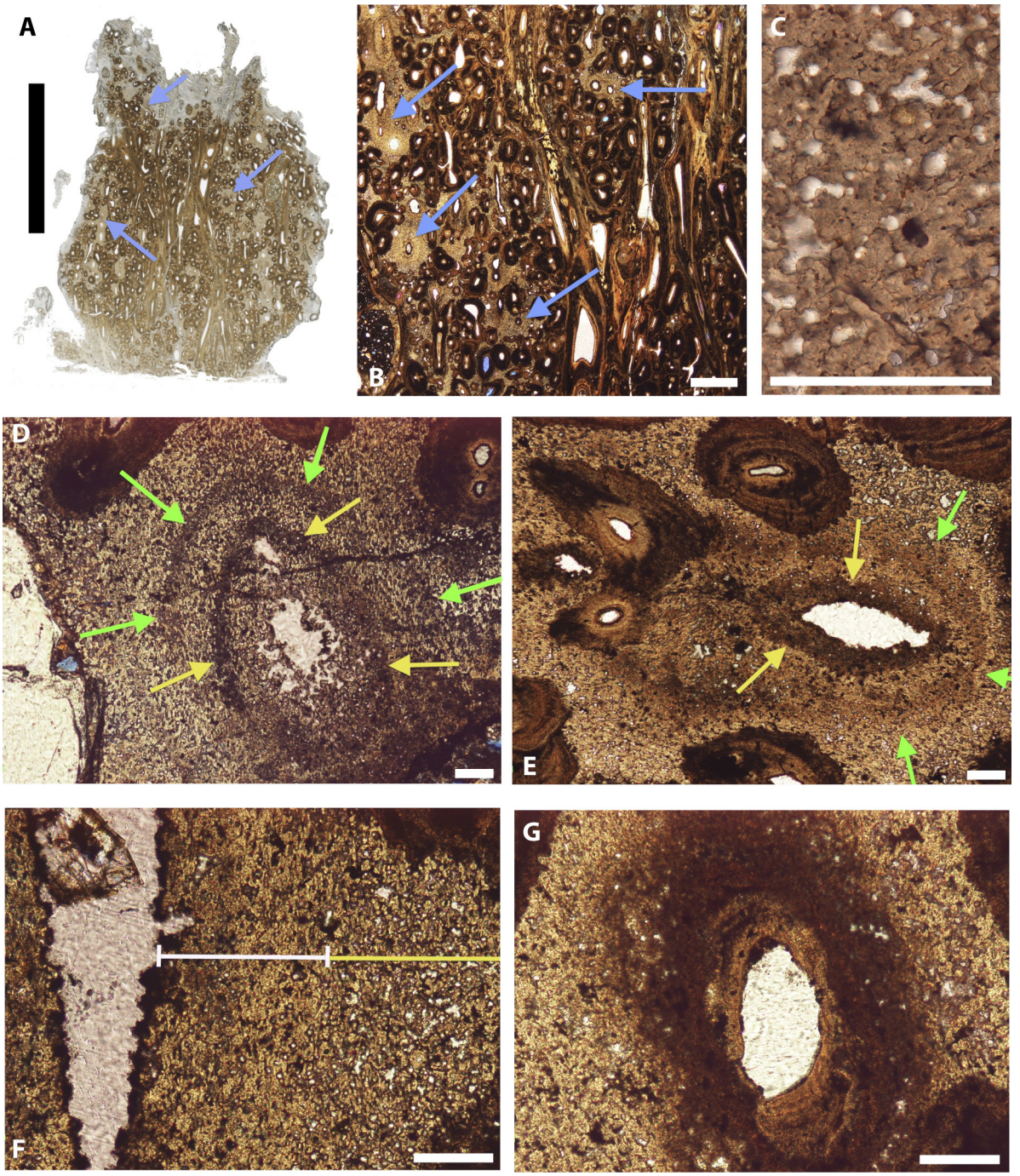

Fig. 8. (Color online.) Coronal sections from the caudal side of a young *Diplodocus* caudal neural spine (MOR592.NS1-L3) (A, B, E, G), (MOR592.NS1-L6) (C), (MOR592.NS1-L4) (D, F). A. Whole section showing primary tissues (blue arrows). Note the dorso-ventral orientation of the centrally located secondary reconstructions. B. Magnified view of A, showing how the primary tissues and secondary reconstructions are interrelated. C. Highly magnified image of the primary tissues showing numerous round empty spaces between what appear to be mineralized tissues. D. Concentric, parallel dark and light colored zones (outer green arrows and inner yellow arrows) surrounding an open area where mineralized tissue looks as if it was breaking up. E. Vascular space surrounded by concentric dark and light zones. Note that the outer edge (green arrows) is not distinct, but simply a different color. F. Magnified area adjacent to a primary vascular space showing that the majority of rounded spaces (seen in C), located nearest the vascular canal (white line) have a dark colored infilling whereas those beyond (yellow line) are mostly empty giving the two zones slightly different colors. G. Vascular space surrounded by a dark reddish zone that has no distinct exterior border. The interior border of the vascular canal is defined by a tissue that appears to be fairly dense. Scale bar in A is 1 cm, in B is 1 mm; all other scale bars are 100 μm.

shows the apparent initial formation of a vascular space. Rather than being tunneled as is typical for osteoclastic resorption, we suggest that the primary tissue was broken down by a combination of phagocytosis and mineral dissolution, likely by a multinucleated macrophage (see Fallon et al., 1983; Young, 1963). We hypothesize that the concentric coloration bands were caused by mineralization of fibrils occupying the rounded spaces in the primary mineral matrix, and as additional spaces were filled and mineralized from the interior outward, the structure became darker in color. Fibroblasts could have deposited fibers along the interior border of the vascular space, thereby causing the internal architecture (i.e., the herring bone organization) we see in Fig. 1H. Once completed this inner rim hypermineralized. Upon completion of the exterior, the edges took on an interdigitated, scalloped appearance due to integration of the rounded fascicles into the edges of the SR. Phagocytosis may also have played a role in the destruction of the endotenon walls as the expanding SR incorporated additional fibers.

We describe the succeeding generations of SRs as this: the youngest SRs (furthest away from the medullary cavity or the center of the bone) possess many fibers separated with arcuate-shaped spaces, while the oldest SRs (i.e., the most internal) appear less fibrous and look like more typical Haversian systems (Fig. 2E) with "normal" looking osteocytes (Fig. 2G). We hypothesize that the temporal sequence of apposition must have undergone a graded, gradual change from fibroblasts to osteoblasts. Moreover, the fact that these tissues and SRs appear acellular (e.g., Figs 2B, 3E, 4D, 5D-F, 6D, 9B) could be due to the fact that these fibroblasts do not adopt an osteoblast-like morphology until later. Only when the SR "matures" and the cells are embedded in the mineralized tissue can they be recognized as osteocytes (*Matthew Vickaryous, personal communication*).

To summarize, the primary tissues apparently formed initially as dense connective tissues and later mineralized through processes of metaplasia. Subsequent to mineralization, phagocytosis occurred, creating open vascular spaces. The concentric banding around each of the SRs may be tide marks indicative of a centripetal mineralization front that eventually incorporated a concentric region of mineralized collagen fibrils within a hypermineralized calcified fibrocartilage matrix.

The *Brachylophosaurus* (MOR 794) ossified tendons described here are constructed primarily of fibrous SRs surrounded by a zone of fibrous primary tissue mostly made up of fascicles. The prezygopophyseal rods of *Deinonychus* (MOR 747), on the other hand, are constructed almost exclusively of individual fibrils and fibrous SRs proximal to the vertebral bases. The lack of obvious vascularization in the distal reaches of the prezygopophyseal rods is interesting in light of several studies suggesting that mineralization of tendons is dependent on vascularization (Landis, 1986; Landis and Arsenault, 1989), prompting Adams and Organ (2005) to hypothesize that the tail rods were simply periosteal extensions of the prezygopophyses. We disagree with this interpretation and suggest instead that the distal tail rods are vascularized, but by much smaller canals than normally seen in typical bone. Most of the tail rods that were examined are vascularized by a central canal, but in cases where they are not, the central area is composed of a lose network of subfascicles with varying sized spaces between (see Fig. 3E). We contend that centralized vascular canals extended a relatively long distance, but then divided into much smaller vesicles that intertwine between the subfascicles. We therefore interpret the formation of tail rods as resulting from metaplasia of dense, elongated connective tissues or fibrocartilage. Interestingly, because the individual tail rods are composed of subfascicles instead of fascicle bundles, these rods are not like ossified tendons or the elongated cervical ribs of sauropods (Cerda, 2009; Klein et al., 2012), but rather more like exceptionally long individual fascicles.

The construction of both the hadrosaur "ossified" tendons and *Deinonychus* prezygopophyseal rods include highly fibrous primary and secondary tissues that not only afforded these structures the rigidity to maintain position of the tail on the sagittal plane (see Ostrom, 1964; Ostrom, 1969; Organ, 2006), but may also have provided flexibility along the transverse plane. Currey (2002) describes ossified tendon (avian) as unique among bony tissues in being "stiff, strong, and tough". The lack of pathologies reported or observed (JRH) in "ossified" tendons (and *Deinonychus* tail rods) even adjacent to vertebral spines that possess pathologies (see Organ, 2006) suggests that these structures had a much different composition than ossified bone and were much more resistant to trauma.

The *Euoplocephalus* (MOR 2010-09) tail club "handle" and nodosaur osteoderm confirms observations of Scheyer and Sander (2004), and supplements them by demonstrating that these highly fibrous tissues are prevalent in much of the skeleton, and likely will be found in additional skeletal elements. Just as Scheyer and Sander (2004) hypothesized that the metaplastic construction of the osteoderm allowed it to be thin and light, yet very strong, the same is true of the tail club "handle": it seems to have been constructed of a very tough, "carbon fiber"-like substance.

Fig. 8. (Couleur en ligne.) Sections coronales au niveau de la partie caudale d'une épine neurale caudale d'un jeune *Diplodocus* (MOR592.NS1-L3) (A, B, E, G), (MOR592.NS1-L6) (C), (MOR592.NS1-L4) (D, F). A. Section entière montrant les tissus primaires (flèches bleues). À noter l'orientation dorso-ventrale des SRs du centre. B. Agrandissement de A montrant les tissus primaires et les RSs interconnectées. C. Agrandissement fort des tissus primaires montrant de nombreux espaces vides entre des tissus apparemment minéralisés. D. Zones concentriques claires et sombres (flèches vertes extérieures et flèches jaunes intérieures) entourant une zone ouverte où le tissu minéralisé semble être en phase de destruction. E. Espaces vasculaires entourés de zones claires et sombres. À noter que le bord extérieur (flèche verte) est indistinct, mais simplement d'une couleur différente. F. Agrandissement de la zone adjacente à un espace vasculaire montrant que la majorité des espaces ronds (vus dans C), localisés près du canal vasculaire (ligne blanche) ont des remplissages foncés, alors que les autres (lignes jaunes) sont vides, ce qui donne des couleurs différentes pour ces deux zones. G. Espaces vasculaires entourés par une zone rougeâtre, sans aucun bord externe discernable. Le bord interne du canal vasculaire est défini par un tissu apparemment assez dense. Les barres d'échelle dans A et B représentent 1 cm et 1 mm respectivement, toutes les autres représentent 100 μm.

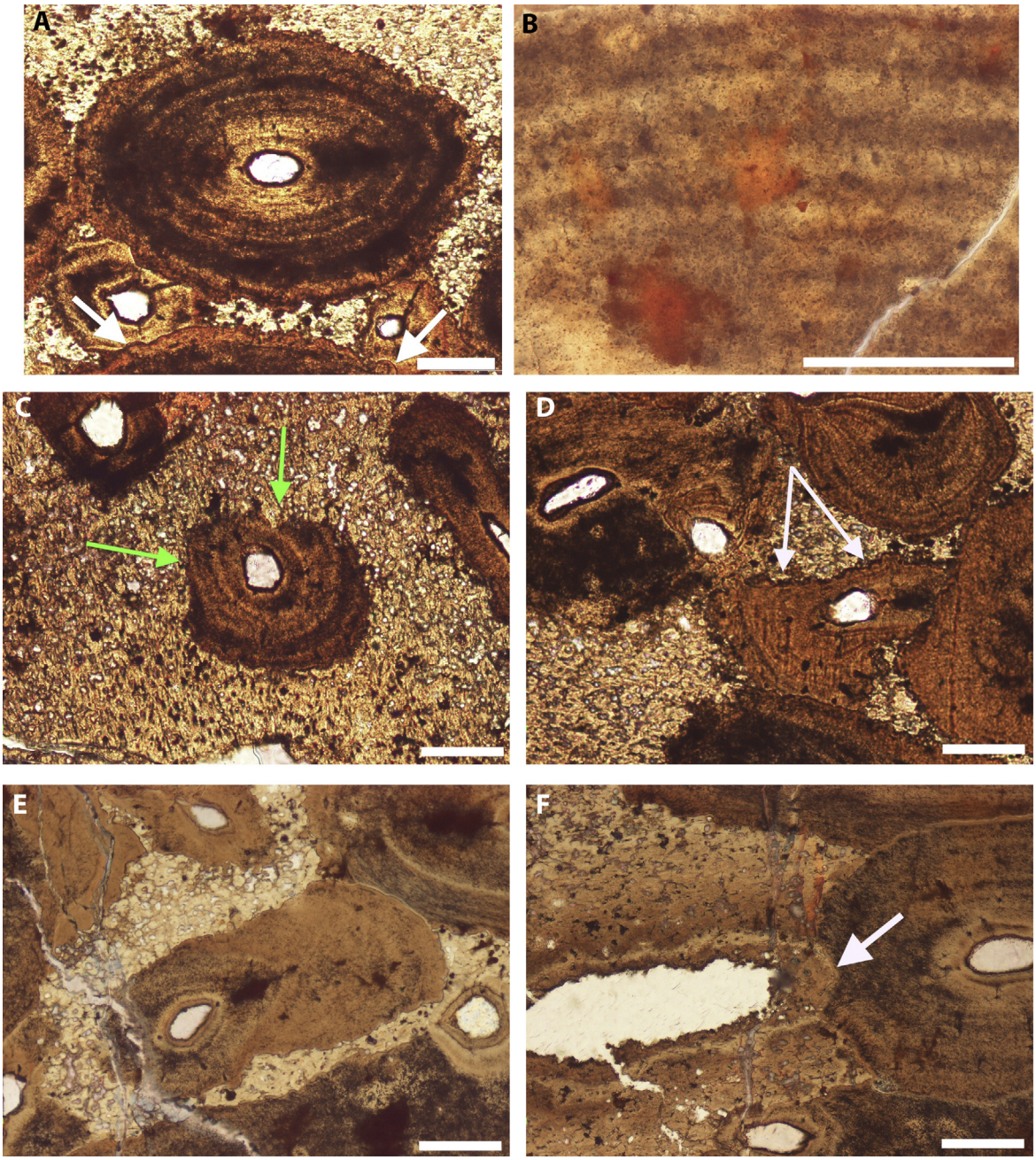

Fig. 9. (Color online.) Coronal sections from the caudal side of a *Diplodocus* caudal neural spine (MOR592.NS1-L3) (A–G). A. Fully-formed secondary reconstruction. Note the ragged exterior edge. B. Highly magnified secondary reconstruction showing the light and dark banding. C. Secondary reconstruction that appears to have sustained some destruction (arrows). D. Secondary reconstruction that has sustained some destruction and deformation. E. Secondary reconstruction that has sustained destruction in areas where it is surrounded by primary tissues, but seems intact where it meets another secondary reconstruction. F. A newly forming SR (left) has invaded (arrow) a portion of a more mature SR (right). All scale bars are 100 μm.

Fig. 9. (Couleur en ligne.) Sections coronales au niveau de la partie caudale d'une épine neurale caudale de *Diplodocus* (MOR592.NS1-L3) (A–G). A, RS complètement formée. À noter la bordure externe irrégulière. B. Agrandissement fort de la RS montrant les bandes claires et sombres. C. Restes de RS ayant été soumis à une sorte de destruction (flèche). D. Restes de RS ayant été soumis à des déformations et destructions. E. Restes de RS ayant été soumis à une sorte de destruction au niveau des tissus primaires. Cependant, cette RS semble être intacte aux endroits où elle est en contact avec une autre RS. F, RS se formant (à gauche) et envahissant une portion (flèche) d'une RS plus mature (à droite). Toutes les barres d'échelle représentent 100 μm.

It was surprising to find similar tissues in the dorsal surface of the nasal of *Prosaurolophus* (MOR 553PN) as this element does not seem as though it would require the same type of strength as that of tendons, tail club handles, or osteoderms. It is certainly true, however, that a fibrous, mineralized construction of the hollow crests of lambeosaurid hadrosaurs would be advantageous considering that some regions of the premaxillae and nasals contributing to the so-called "resonating chambers" are often less than 5 mm in thickness. Another possibility is that stress and strain are directed in the nasals of *Prosaurolophus* during feeding, just like they are in *Tyrannosaurus rex* (Rayfield, 2004). Indeed, Rayfield (2004) found that *T. rex* was adapted to resist biting and tearing forces through the open maxillajugal suture that reduced tension in the ventral skull. As a consequence of reducing tension in this part, the stresses and strains were directed to the nasals, explaining why *T. rex* nasals are often robust. Perhaps a similar process occurs in *Prosaurolophus*, and very hard metaplastic tissues in the nasals might have been advantageous for resisting stress and strain. It will be interesting to section other cranial elements from a wider variety of dinosaurs (such as *T. rex*) to see if we can find additional skull bones sharing this quality.

Unlike the dense connective tissues mineralized via metaplasia within tendons, tail rods, and cranial elements, the mineralized nuchal ligament tissues located between the tidemark and enthesis of dinosaur vertebrae appear to be hypermineralized calcified fibrocartilage (Figs. 7–9). These tissues are similar to most, if not all, junctions of hypermineralized calcified fibrocartilage and bone in extant vertebrates (see Shea et al., 2001). However, there remains the question of the actual consistency of the "bony" SR tissues in which the hypermineralized calcified fibrocartilage interdigitates. As with the other dinosaurian examples, and unlike typical secondary osteons, the SRs within the vertebral enthesis are composed of dense fibers (Fig. 9G) and are likely formed identical to all other fibrous SRs.

5. Conclusions

It is not surprising that the "ossified" tendons of some hadrosaurs, the prezygopohyseal tail rods of dromaeosaurids, and the osteoderms and tail handles of ankylosaurs appear to have originated from tendon-like structures, that subsequently mineralized through a process of metaplasia, considering the various biomechanical functions proposed for these structures (see Organ and Adams, 2005; Organ, 2006; Hayashi et al., 2010). Surprising is the discovery that similar tissues apparently formed a portion of the *Prosaurolophus* nasal. Skeletal tissues mineralized via processes of metaplasia may be significantly more prevalent in dinosaurs than previously considered, and may account for other cranial and postcranial ornamental features. It could be that the "carbon fiber"-like composition of these dense fibrous tissues provided the necessary rigidity and strength required for the activities in which these animals may have used their ornamental features.

The enthesial fibrocartilage of the sauropod presents metaplastic characteristics as well, and it is not surprising because entheses are known to be sites for metaplastic transformations in extant species. Although a metaplastic transformation is expected at these boundaries, what was discovered during this study was a possible explanation for the highly fibrous SRs. The SRs in these highly fibrous tendinous-like structures and the fibrocartilage appear to have initially formed without the activity of osteoclasts or osteoblasts. The opening of a secondary vascular space may have formed via cellular enzymatic lysis.

The most peripheral SRs are the most fibrous, and those found deeper in the tendinous structures are found to be more like "normal" Haversian systems, suggesting an ontogenetic sequence. It is therefore evident that a new study will need to be conducted on an ontogenetic series of ossified tendons in extant avian taxa, in order to identify precursor tissues and the process(es) by which secondary vascular spaces are formed.

Acknowledgments

We thank Ellen-Thérèse Lamm and Christian Heck at the Gabriel Laboratory for Cellular and Molecular Paleontology (Museum of the Rockies) for making the dinosaur thin sections. We are grateful to Armand De Ricqlès and Susan Gibson for fruitful discussions. We also thank Matthew Vickaryous for his extremely helpful insights and knowledge on metaplastic transformations in *Alligator mississippiensis*. We are indebted to Elizabeth Moore and the Museum of the Rockies for funding. Finally, we thank Michel Laurin and Jorge Cubo for inviting us to this thematic issue of *C. R. Palevol*, and Torsten Scheyer and Shoji Hayashi for their helpful reviews.

Appendix A. Supplementary data

Supplementary data associated with this article can be found, in the online version, at http://dx.doi.org/10.1016/j.crpv.2015.01.006.

References

Abdalla, O., 1979. Ossification and mineralization in the tendons of the chicken (*Gallus domesticus*). J. Anat. 129, 351–359.
Adams, J.S., Organ, C.L., 2005. Histologic determination of ontogenetic patterns and processes in hadrosaurian ossified tendons. J. Vertebr. Paleontol. 25, 614–622.
Araya, J.S., Cambier, S.A., Markovics, J.A., Wolters, P., Jablons, D., Hill, A., Finkbeiner, W., Jones, K., Broaddus, V.V., Sheppar, D., 2007. Squamous metaplasia amplifies pathologic epithelial-mesenchymal interactions in COPD patients. J. Clin. Invest. 117, 3551–3562.
Beresford, W.A., 1981. Chondroid Bone, Secondary Cartilage and Metaplasia. Urban & Schwarzenberg, Inc., Baltimore, MD, USA.
Cerda, I.A., 2009. Consideraciones sobre la histogénesis de las costillas cervicales en los dinosaurios saurópodes. Ameghiniana 46, 1–8.
Coombs, W.P., 1995. Ankylosaurian tail clubs of Middle Campanian to Early Maastrichtian age from western North America, with description of tiny club from Alberta and discussion of tail orientation and tail club function. Can. J. Earth Sci. 32, 902–912.
Currey, J.D., 2002. Bones: Structure and Mechanics, Second Edition. Princeton University Press, Princeton, NJ, USA.
de Ricqlès, A., Padian, K., Horner, J.R., 2001. The bone histology of basal birds in phylogenetic and ontogenetic perspectives. New Perspectives on the Origin and Early Evolution of Birds, New Haven, CT, USA.

Eguchi, G., 1976. "Transdifferentiation" of vertebrate cells in cell culture. In: Elliott, K., O'Connor, M. (Eds.), Embryogenesis in Mammals. American Elsevier, New York, pp. 241–258.
Fallon, M.D., Teitelbaum, S.L., Kahn, A.J., 1983. Multinucleation enhances macrophage-mediated bone resorption. Lab. Invest. 49, 159–164.
Francillon-Vieillot, H., de Buffrénil, V., Castanet, J., Geraudie, J., Meunier, F.J., Sire, J.Y., Zylberberg, L., de Ricqlès, A., 1990. Microstructure and mineralization of vertebrate skeletal tissues. In: Carter, J.G. (Ed.), Skeletal Biomineralization: Patterns, Processes and Evolutionary Trends, 1. Van Nostrand Reinhold, New York, pp. 471–548.
Goodwin, M.B., Horner, J.R., 2004. Cranial histology of pachycephalosaurs (Ornithischia: Marginocephalia) reveals transitory structures inconsistent with head-butting behavior. Paleobiology 30, 253–267.
Haines, R.W., 1969. Epiphyses and sesamoids. In: Gans, C. (Ed.), Biology of the Reptilia. Academic Press, New York, pp. 81–115.
Haines, R.W., Mohuiddin, A., 1968. Metaplastic bone. J. Anat. 103, 527–538.
Hall, B.K., 2005. Bones and cartilage: developmental and evolutionary skeletal biology. Elsevier Academic Press, San Diego, CA, USA.
Hayashi, S., Carpenter, K., Scheyer, T.M., Watabe, M., Suzuki, D., 2010. Function and evolution of ankylosaur dermal armor. Acta Palaeontol. Pol. 55, 213–228.
Horner, J.R., Makela, R., 1979. Nest of juveniles provides evidence of family structure among dinosaurs. Nature 282, 296–298.
Horner, J.R., Goodwin, M.B., 2009. Extreme cranial ontogeny in the Upper Cretaceous dinosaur *Pachycephalosaurus*. Plos One 4, e7626.
Horner, J.R., Lamm, E.T., 2011. Ontogeny of the parietal frill of *Triceratops*: a preliminary histological analysis. C. R. Palevol 10, 439–452.
Klein, N., Christian, A., Sander, P.M., 2012. Histology shows that elongated neck ribs in sauropod dinosaurs are ossified tendons. Biol. Lett., http://dx.doi.org/10.1098/rsbl.2012.0778.
Lamm, E.-T., 2013. Chapter 4: Preparation and Sectioning of Specimens. In: Padian, K., Lamm, E.T. (Eds.), Bone Histology of Fossil Tetrapods: Advancing Methods, Analysis, and Interpretation. University of California Press, Berkeley, CA, USA, pp. 55–160.
Landis, W.J., 1986. A study of calcification in the leg tendons from the domestic turkey. J. Ultrastruct. Mol. Struct. Res. 94, 217–238.
Landis, W.J., Arsenault, A.L., 1989. Vesicle- and collagen-mediated calcification in the turkey leg tendon. Connect. Tissue Res. 22, 661–668.
Landis, W.J., Silver, F.H., 2002. The structure and function of normally mineralizing avian tendons. Comp. Biochem. Physiol. A 133, 1135–1157.
Landis, W.J., Kraus, B.L., Kirker-Head, C.A., 2002. Vascular-mineral spatial correlation in the calcifying turkey leg tendon. Connect. Tissue Res. 43, 595–605.
Levrat-Calviac, V., Zylberberg, L., 1986. The structure of the osteoderms in the Gekko: *Tarentola mauritanica*. Am. J. Anat. 176, 437–446.
Main, R.P., de Ricqlès, A., Horner, J.R., Padian, K., 2005. The evolution and function of thyreophoran dinosaur scutes: implications for plate function in stegosaurs. Paleobiology 31, 291–314.
Moodie, R.L., 1928. The histological nature of ossified tendons found in dinosaurs. Am. Mus. Novitat. 311, 1–15.
Moss, M.L., 1969. Comparative histology of dermal sclerifications in reptiles. Acta Anat. 73, 510–533.
Organ, C.L., 2006. Biomechanics of ossified tendons in ornithopod dinosaurs. Paleobiology 32, 652–665.
Organ, C.L., Adams, J., 2005. The histology of ossified tendon in dinosaurs. J. Vertebr. Paleontol. 25, 602–613.
Ostrom, J.H., 1964. A reconsideration of the paleoecology of hadrosaurian dinosaurs. Am. J. Sci. 262, 975–997.
Ostrom, J.H. (Ed.), 1969. Osteology of Deinonychus antirrhopus an unusual theropod from the Lower Cretaceous of Montana, 30. Peabody Museum of Natural History, New Haven, CT, USA.
Parks, W.A., 1924. *Dyoplosaurus acutosquameus*, a new genus and species of armored dinosaur; and notes on skeleton of *Prosaurolophus maximus*. Univ. Toronto Geol. Ser. 18, 5–35.
Rayfield, E.J., 2004. Cranial mechanics and feeding in *Tyrannosaurus rex*. Proc. Royal Soc. Lond., Series B: Biol. Sci. 271, 1451–1459.
Reid, R.H., 1996. Bone histology of the Cleveland–Lloyd dinosaurs and of dinosaurs in general; part I: Introduction: Introduction to bone tissues. BYU Geol. Stud. 41, 25–71.
Rooney, P., 1994. Intertendinous ossification. In: Hall, B.K. (Ed.), Bone. Mechanisms of Bone Development and Growth, 8. CRC Press, Boca Raton, FL, USA, pp. 47–84.
Scheyer, T.M., Sander, P.M., 2004. Histology of ankylosaur osteoderms: implications for systematics and function. J. Vertebr. Paleontol. 24, 874–893.
Scheyer, T.M., Martin Sander, P., Joyce, W.G., Böhme, W., Witzel, U., 2007. A plywood structure in the shell of fossil and living soft-shelled turtles (Trionychidae) and its evolutionary implications. Org. Divers. Evol. 7, 136–144.
Shea, J.E., Vajda, E.G., Bloebaum, R.D., 2001. Evidence of a hypermineralized calcified cartilage on the human femoral neck and lesser trochanter. J. Anat. 198, 153–162.
Ten Cate, A.R., 1972. Morphological studies of fibrocytes in connective tissue undergoing rapid remodeling. J. Anat. 112, 401–414.
Vanden Berge, J.C., Storer, R.W., 1995. Intratendinous ossification in birds: a review. J. Morphol. 226, 47–77.
Vickaryous, M.K., Hall, B.K., 2008. Development of the dermal skeleton in *Alligator mississippiensis* (Archosauria, Crocodylia) with comments on the homology of osteoderms. J. Morphol. 269, 398–422.
Witten, P.E., Villwock, W., 1997. Growth requires bone resorption at particular skeletal elements in a teleost fish with acellular bone (*Oreochromis niloticus*, Teleostei: Cichlidae). J. Appl. Ichthyol. 13, 149–158.
Young, R.W., 1963. Histophysical studies on bone cells and bone resorption. In: Sognnaes, R.F. (Ed.), Mechanisms of Hard Tissue Destruction. American Association for the Advancement of Science, Washington DC, pp. 471–496.